Comparative analysis of day and night micronekton abundance estimates in west Pacific between acoustic and trawl surveys

Laure Barbin, Anne Lebourges-Dhaussy, Valérie Allain, Aurore Receveur, Patrick Lehodey, Jérémie Habasque, Elodie Vourey, Annie Portal, Gildas Roudaut, Christophe Menkes

Comparative analysis of day and night micronekton abundance estimates in west pacific between acoustic and trawl surveys

Barbin Laure [1, 2, *], Lebourges-Dhaussy Anne [2], Allain Valerie [3], Receveur Aurore [4], Lehodey Patrick [3, 5], Habasque Jeremie [2], Vourey Elodie [3], Portal Annie [3], Roudaut Gildas [2], Menkes Christophe [1]

[1] ENTROPIE, UMR 9220, IRD, Univ. de La Réunion, CNRS, 101 Promenade Roger Laroque, 98800, Noumea, New Caledonia
[2] IRD, University of Western Brittany, CNRS, Ifremer, LEMAR, Campus Ifremer, BP70, 29280, Plouzané, France
[3] OFP/FAME Division, Pacific Community, 95 Promenade Roger Laroque, BP D5, 98848, Noumea, New Caledonia
[4] CESAB - FRB, 5 Rue de L'École de Médecine, 34000, Montpellier, France
[5] Mercator Ocean International, Toulouse, France

* Corresponding author : Laure Barbin, email address : laure.barbin@ird.fr

Abstract :

Micronekton organisms are a central component of the trophic organization in the pelagic ecosystem, being prey to top predators and participating in the export of carbon from the surface to the deep layers. Despite their importance, the abundancedeep sea estimates and species distribution of micronekton remain largely uncertain. This study aimed to compare and assess two sampling methods classically used for the estimation of micronekton abundance in mesopelagic acoustic scattering layers: scientific echosounder and trawl sampling. Measurements of 38 and 70 kHz hull-mounted echosounders were examined with biological trawl samples from 8 surveys in the South-West tropical Pacific. A model of acoustic observation was built from the trawl sampling species composition and forward scattering models. Predicted and observed acoustic responses are compared to assess the variability and the difference between the acoustic and trawl sampling methods in various scattering layers, for day and night periods. The difference between methods decreased with depth and with increasing abundance of fish with swimbladders caught in trawls. Notably, this difference was found to be minimal in the nocturnal deep scattering layer (mesopelagic zone, depth>200 m). This study emphasizes potential lower estimates of organisms' abundance by trawling and a bias towards mesopelagic fish. Understanding the differences between methods and their variability within different scattering layers is essential for studying micronekton and improving the precision of biomass estimates.

Highlights

► Acoustic-trawl surveys in scattering layers of West tropical Pacific. ► Forward scattering models applied to micronekton trawl sampling with a high species diversity. ► The difference in micronekton density estimates between acoustic and trawl methods varies across scattering layers. ► The disparities between methods decrease in night mesopelagic layers and trawls with high swimbladdered fish density.

Introduction

Micronekton, ubiquitous to all oceans and distributed in mesopelagic acoustic scattering layers plays a pivotal role in the trophic organisation of the pelagic ecosystem. It feeds on zooplankton and serves as prey for mid-level and top predators, including tuna (Bertrand et al., 2002; Young et al., 2015).

35   Micronekton are defined by a size range from 2 to 20 cm and encompasses a large variety of species

36   that can be classified into large taxonomic categories: fishes including mesopelagic fish, crustaceans,

37   gelatinous organisms, and molluscs (including squids) (Blackburn, 1968; Brodeur et al., 2004; Escobar-

38   Flores et al., 2019). A significant portion of species of micronekton, which has been estimated to be

39   78% in the Coral Sea (Receveur et al., 2020a), undertakes a diel vertical migration (DVM). They migrate

40   from the deeper layers (200-1000m), where they reside during the daytime, to the surface layers

41   (epipelagic: 0-200m or upper-mesopelagic: 200-500m) at night (Pearre, 2003; Brierley, 2014; Czudaj et

42   al., 2021). This migration pattern contributes to the biogeochemical fluxes between the surface and

43   the mesopelagic domain (Davison et al., 2013; Ariza et al., 2015; Anderson et al., 2019). The frequent

44   distribution of micronekton in dense scattering layers in the upper 1000m of the water column varying

45   with time and space (Burgos and Horne, 2008; Benoit-Bird and Lawson, 2016) poses challenges for

46   their study.

47   Micronekton, with their significant contribution to the overall biomass of the oceans, present a

48   challenge for accurate biomass estimates due to their high species diversity. Estimates often focus

49   more specifically on a taxonomic group, such as mesopelagic fish or krill. When considering

50   mesopelagic fish biomass, trawl sampling provides the lowest estimate around 1 billion tons (Gjøsæter

51   and Kawaguchi, 1980). Acoustic studies show median estimates between 3.8 and 15 billion tons

52   (Irigoien et al., 2014). Proud et al. (2019) further refines this range to 3.8 to 8.3 billion tons, accounting

53   for factors like the proportion of mesopelagic fish without gas-filled inclusion and the contribution of

54   other micronekton organisms. Additionally, ecosystem-based trophic models bridge the gap between

55   acoustic studies and historical trawl sampling estimates, predicting a mesopelagic fish biomass of 2.4

56   billion tons (Anderson et al., 2019), which is 26 to 130% higher than Hill Cruz et al. (2023) estimates.

57   The significant variability in biomass estimates of mesopelagic fish and the difficulty to include all

58   taxa of micronekton can be attributed to biases inherent to each of the two methods. The acoustic

59   provides a proxy of the density of organisms throughout the water column and the single narrowband

60   38kHz is commonly employed to investigate the biomass of mid-trophic organisms, particularly

61   mesopelagic fishes, within the depth range from the surface down to 1000 meters (Kloser et al., 2009;

62   De Robertis et al., 2017b; Receveur et al., 2020a). Interpreting the backscattered volume using this

63   single frequency is quite challenging in ecosystems characterized by a wide diversity of taxa and mixed

64   scattering layers. Dominant scatterers, which include organisms with gas-filled inclusions, tend to mask

65   the response of the weaker scatterers, such as crustaceans and fish lacking gas-bladder (Mair et al.,

66   2005; Davison et al., 2015; Dornan et al., 2019, 2022). Furthermore, the target strength (TS), which

67   represents the individual acoustic response of organisms, varies depending on their size and

68   orientation within a species (McGehee et al., 1998; Scoulding et al., 2017). The insonified volume

69   increases with the distance to the echosounder, thereby potentially increasing the number and

70 diversity of the scattering organisms' taxa detected with depth in the mean backscattered response,

71 further complicating its interpretation.

72 Regarding the pelagic trawl sampling method, it is an essential tool to collect biological samples

73 from specific depth layers in order to assess the taxonomic diversity of organisms (Receveur et al.,

74 2020b). However, relying solely on this method for estimating the abundance of mesopelagic

75 organisms introduces biases, primarily due to avoidance behaviour exhibited by nektonic organisms

76 (Kaartvedt et al., 2012), variable catchability among species (Arreguín-Sánchez, 1996; De Robertis et

77 al., 2017; Underwood et al., 2020) and selectivity associated with trawl mesh size (Heino et al., 2011;

78 Grimaldo et al., 2022).

79 Therefore, examining the acoustic backscatter in conjunction with *in situ* biological sampling is

80 essential for accurate estimation of micronekton density and diversity (McClatchie et al., 2000).

81 Understanding the morphological characteristics of species within scattering layers (Kloser et al., 2009;

82 Dornan et al., 2022) enables the investigation of their contributions to the acoustic backscattered

83 signal (Scoulding et al., 2017). Combined acoustic-trawls studies have demonstrated successful

84 estimation of mesopelagic fish biomass in ecosystems with low species diversity (De Robertis et al.,

85 2017b; Scoulding et al., 2017). However, the uncertainty in biomass estimates tends to increase with

86 the biodiversity in ecosystems. There is uncertainty regarding whether trawls tend to underestimate

87 the abundance of organisms and fail to provide a homogeneous sampling of all species (Mair et al.,

88 2005; Kloser et al., 2009; Blanluet et al., 2019). Although imperfect, trawls remain essential for

89 understanding the composition of scatterers in ecosystems, and in particular the proportion of weak

90 and strong scatterers (Dornan et al., 2022). Due to the paucity of sampling and inherent biases

91 associated with trawl and acoustic methods, precise estimations of the abundance and species

92 distribution of micronekton organisms remain highly uncertain when accounting for all taxa (St. John

93 et al., 2016; Hidalgo and Browman, 2019; Fjeld et al., 2023). This is particularly the case for mesopelagic

94 communities in the tropical Pacific (Klevjer et al., 2020; Ariza et al., 2022), further amplifying the

95 uncertainty regarding micronekton abundance.

96 The present study aims at interpreting acoustics at 38 and 70 kHz relative to trawl sampling in

97 the tropical southwest Pacific. Comparison of acoustics and biological sampling is achieved through

98 forward method, which converts trawl species composition and abundances into volume backscatter.

99 This method uses theoretical scattering models and biological samplings from midwater trawls

100 collected during 8 surveys providing species densities, sizes and distributions (e.g. Blanluet et al., 2019).

101 This approach predicts the theoretical mean volume backscattered signal in the scattering layers,

102 considering all captured taxa, and compares it to the mean volume backscatter from the hull-mounted

103 echosounder. The disparities between the two acoustic densities in relation to the time-period,

104 sampling depth and trawl composition were explored within various scattering layers. This study

105 highlights the complexity of estimating micronekton densities in environments with high biodiversity,
106 and the need to resolve the main causes of discrepancies between these two complementary
107 observation methods to better estimate biomass and clarify the uncertainty on this estimate.

108 **1. Materials and methods**

109 Data used in this paper were collected during eight research cruises spanning 2011-2021 (Nectalis
110 1-5, Wallalis, KANARECUP and WARMALIS-1, referred to as NEC1-5, WAL, KANA and WARM) in the
111 western tropical Pacific region (Figure 1, Table 1). The cruises covering the area between 157°E-176°W
112 and 4°N-26°S were conducted on board R/V Alis (French oceanographic fleet) with the objective of
113 understanding the mechanisms structuring the pelagic ecosystem that supports tuna fisheries in the
114 region. All surveys included hull-mounted narrowband data and micronekton trawl sampling, where
115 the acoustic recordings and trawls were conducted simultaneously.

116
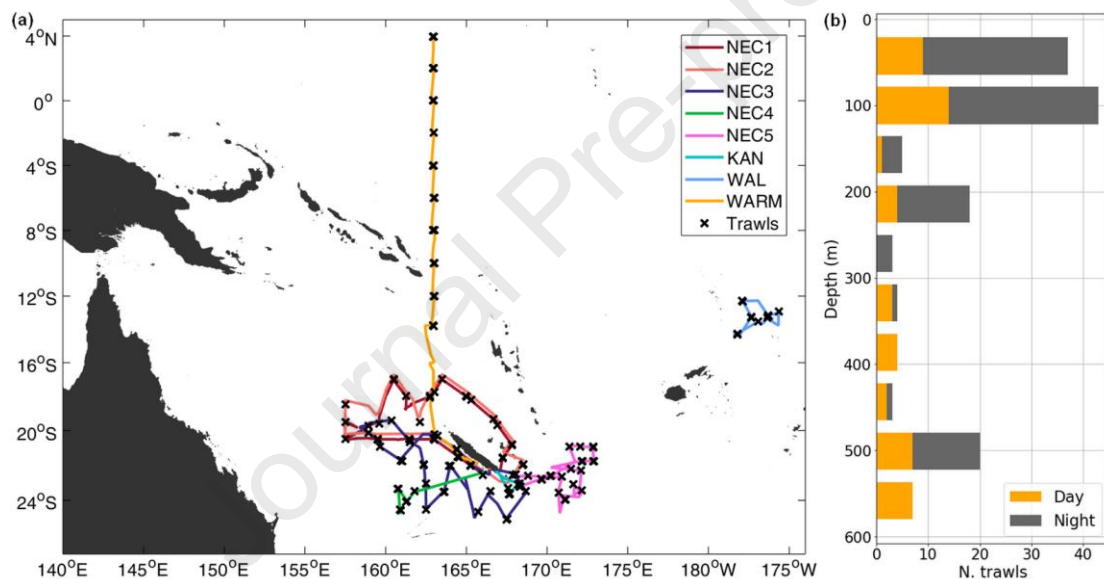
117 **Figure 1.** Map of the south-western Pacific Ocean, showing (a) cruise tracks with the R/V Alis. NEC1 and NEC2
118 tracks partially overlap. The NEC2 track was therefore artificially shifted to the north for visualization purposes.
119 Black crosses represent trawl sampling stations. Dark grey areas illustrate lands above sea surface level. (b)
120 Number of trawls per depth colored by time of the day. Depth refers to the average towing depth during fishing.

121

122 **Table 1.** Details of the 8 cruises aboard R/V Alis, with the cruise name, start and end dates, locations and number
123 of trawls used in this study. EEZ is for Economic Exclusive Zone.

Cruise name	Time Period	Location	Number of trawls
Nectalis 1 [a]	30/07/2011 – 15/08/2011	New-Caledonia EEZ	15
Nectalis 2 [b]	26/11/2011 – 14/12/2011	New-Caledonia EEZ	25
Nectalis 3 [c]	21/11/2014 – 08/12/2014	New-Caledonia EEZ	26
Nectalis 4 [d]	19/10/2015 – 25/10/2015	New-Caledonia EEZ	8
Nectalis 5 [e]	23/11/2016 – 06/12/2016	New-Caledonia EEZ	30
Wallalis [f]	01/07/2018 – 16/07/2018	Wallis-and-Futuna EEZ	11
Kanarecup [g]	19/12/2020 – 11/05/2021	New-Caledonia EEZ	7

4

| Warmalis 1 [h] | 06/09/2021 – 03/10/2021 | West tropical Pacific Ocean | 22 |

124 a. Allain and Menkes (2011a), b. Allain and Menkes (2011b), c. Allain and Menkes (2014), d. Allain and Menkes
125 (2015), e. Allain and Menkes (2016), f. Allain and Menkes (2018), g. Olu and Allain (2020), h. Menkes and Allain
126 (2021).

127 **1.1 Acoustic data**

128   Acoustic narrowband data at 38 and 70 kHz were recorded continuously with a calibrated
129 (Foote et al., 1987; Demer et al., 2015) hull-mounted EK60 echosounder (SIMRAD Kongsberg Maritime
130 AS, Horten, Norway) using two split-beam transducers. The sounder was located at 3.1m below the
131 surface. The acquisition and calibration parameters are described in Supplementary Table S1. The
132 water column was sampled down to 800 m and 400 m depth for 38 and 70 kHz, respectively, except
133 for NEC1, where the range was limited at 600 m for the 38 kHz.

134   The raw acoustic data were pre-processed using the open source tool "Matecho" (Perrot et
135 al., 2018) developed by the French National Research Institute for Sustainable Development (IRD),
136 which incorporates the "Movies3D" software developed at the French Research Institute for
137 Exploitation of the Sea (IFREMER; Trenkel et al., 2009). The pre-processing steps followed the
138 procedures described in Receveur et al. (2020a). The volume backscattering strength was then echo-
139 integrated between 8 and 600 m depth onto 1 m depth interval over an Elementary Distance Sampling
140 Unit (EDSU) of 0.1 nmi, with a -100 dB threshold. The acoustic mean volume backscattering strength
141 S_v (in dB re 1 m^{-1}) was calculated as $S_v=10 \log(s_v)$, with s_v the volume backscattering coefficient in m$^{-$
142 ^{1} (MacLennan et al., 2002). Migration periods (dusk and dawn) were excluded by considering the solar
143 elevation angle, removing EDSU with an altitude angle between 0° and 18° (Lehodey et al., 2015).

144   **Mean S_v in trawled scattering layers.** At each trawl station, the average S_v was determined
145 from the echosounder within the sampled layer by overlaying trawl tracks onto echo-integrated
146 echograms (Figure 2). As the trawl was towed behind the vessel, acoustic data were not exactly
147 simultaneously recorded during trawling. The offset time of the trawl relative to the echosounder was
148 adjusted by using the mean vessel speed over the tow and computing the trawl wire length at the
149 maximum towing depth. The S_v values were extracted along the trawl track within the towing depth
150 layer interval indicated by the solid lines in Figure 2 and averaged (in the linear domain) to obtain the
151 mean $S_{v,obs}$ for trawl. The areas of hauling and setting (Figure 2, dashed lines) were excluded of $S_{v,obs}$.
152 Sampling depth of each trawl was estimated as the mean depth during towing and referred as d_{trawl}.

153
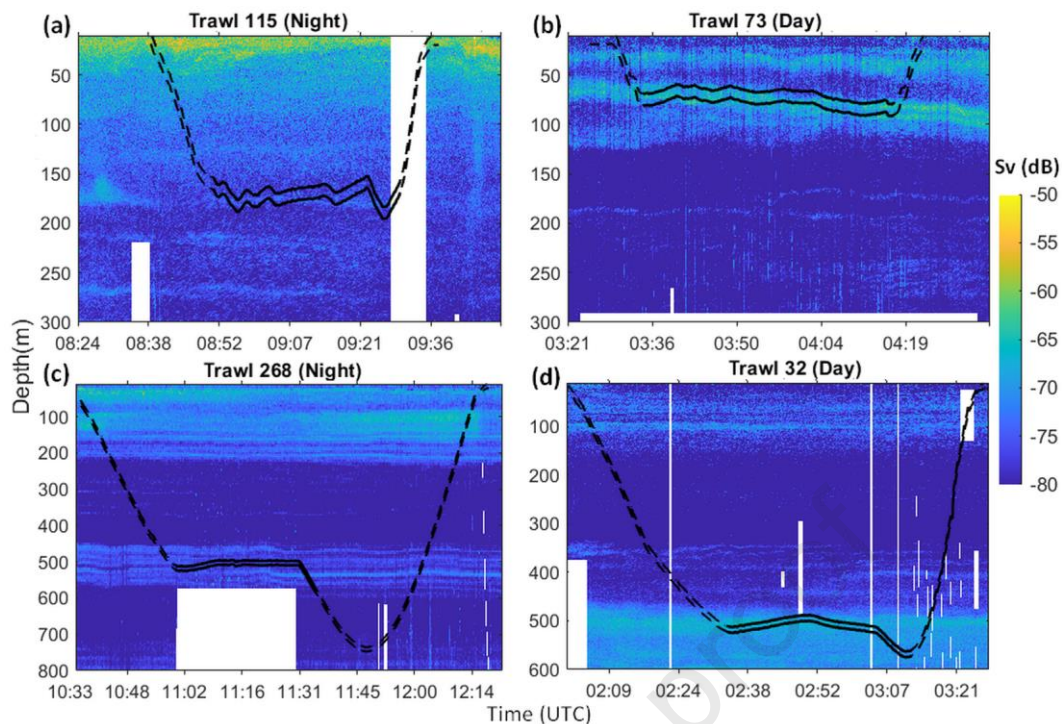
Figure 2. Examples of extraction of $S_{v,obs}$ during trawling at 38 kHz. Echogram from EK60 at 38 kHz acquired while trawling in the epipelagic layer: (a) trawl #115 (night-time, during NEC5) and (b) #73 (day-time, during NEC3) and in the mesopelagic layer: (c) trawl #268 (night, during WARM) and (d) #32 (day, during NEC2). The colorscale indicates the mean volume backscattering strength (S_v in dB re 1 m^{-1}). The trawl track is shown in black lines. The solid lines indicate the towing layer when fishing, used to calculate d_{trawl} and compute $S_{v,obs}$, while the dotted line represents the setting and hauling periods. White areas show acoustic data excluded during pre-processing.

1.2 Micronekton trawl sampling

A total of 190 small pelagic mid-water trawls were conducted during the 8 campaigns (Figure 1). The trawl had a length of 55m and a mesh size that gradually decreased from 80mm at the mouth to 10mm at the cod-end. The average vertical and horizontal opening of 10m were monitored during trawling, along with depth using four acoustic-net-monitoring systems (Scanmar AS, SS4 Depth Sensor) attached to the headline, footrope and wings of the net. Prior to each trawl, the target depth was determined based on real-time analysis of acoustic data, aiming to target the scattering layers with the highest acoustic density. Once stabilized at the selected depth, the trawl was towed horizontally for 30 minutes at an average speed of 3 knots. All trawls were conducted similarly, at the exception of the epipelagic trawls (d_{trawl}<200 m) during WARM, where oblique tows were performed between the surface and 200 m depth. On board the vessel, biological samples were sorted by broad taxon (e.g. fishes, crustaceans, cephalopods and gelatinous organisms), before being frozen at -20°C. In the laboratory at the Pacific Community (SPC), the thawed specimens were counted, weighted, and further examined to identify the species. While we aimed to identify specimens to the more precise taxon possible, gelatinous organisms, in particular, were challenging to identify accurately due to the damage caused by trawling and the difficulty of identification after thawing. Siphonophores, being colonial

6

176 organisms that may be separated during trawling, were particularly challenging to count and measure.
177 Therefore, the mean length of siphonophores was not included in the description of acoustic
178 categories in Table 2.

179   To apply forward scattering models to trawl samples, the species were classified into different
180 groups based on their acoustic properties. These groups, referred to as acoustic categories
181 subsequently, included fish with gas-filled swimbladder (abbreviated in fish with swimbladders or
182 SWB), fish without swimbladder, decapods and euphausiids, amphipods, squids, jellyfishes, other
183 gelatinous organisms (abbreviated as gelatinous), elastic-shelled pteropods (abbreviated as shelled
184 pteropods), and siphonophores bearing a pneumatophore (Table 2). Fish were divided in two
185 categories based on the presence or absence of a gas-filled swimbladder, determined from literature
186 and considering their species and developmental stage (see Supplementary S2). When no information
187 was available, the taxa was assigned to the category most represented in its Family (Marohn et al.,
188 2021). Fish without swimbladder included three types of fish: i) species that lack gas-filled inclusions
189 throughout their entire life cycle, 2) adult fish of species that possess a swimbladder only during their
190 juvenile stage while the swimbladder regresses at the adult stage and 3) fish bearing a lipid-invested
191 swimbladder. As a result, depending on the developmental stage of each specimen, a species could be
192 classified in both fish with swimbladders and fish without swimbladder.

193   The density of organisms (ρ_T, in individuals/1000m^3) was calculated for every acoustic
194 category in each trawl. The volume of water sampled by the trawl ($V_{sampled}$) was estimated based on
195 the distance covered by the trawl during fishing and the trawl opening (as in Receveur et al., 2020b).
196 The periods of hauling and setting were not included (see Figure 2). Trawls conducted during migration
197 periods (dusk and dawn) were excluded, accounting for approximately 10% of the total trawls.

198

199 **Table 2.** Description of taxonomic groups used as acoustic categories of specimens sampled with the
200 trawl. The frequency of presence of each categories in all trawls (% trawls), mean length (in mm) and
201 standard deviation, mean weight (in grams) and standard deviation, number of taxa in each category
202 and the two main taxa found in each category in percentage of occurrence in the category and in the
203 total catches were indicated. The more precise taxonomic level of identification is indicated by
204 superscript numbers after taxon names: 1.Genus, 2.Subfamily, 3.Family, 4.Suborder.

Taxonomic group	Presence (% trawls)	Mean length (mm)	Mean wet weight (g)	Taxa richness (N. of taxa)	Two most abundant taxa (% within group, % across group)
Fish with swimbladders	98	42 (21)	189 (280)	310	*Ceratoscopelus warmingii* (33, 12) *Polyipnus* sp. [1] (8, 3)
Fish without swimbladder	98	83 (66)	81 (121)	102	Bathymyrinae [2] (11, 1) *Lobianchia gemellarii* (8, 0.5)
Decapods & Euphausiids	97	28 (10)	23 (34)	109	*Thysanopoda tricuspidata* (19, 3) *Euphausia mucronata* (16, 2)
Amphipods	80	20 (11)	3 (5)	35	*Phronima* sp. [1] (56, 2) *Phronima sedentaria* (15, 0.5)

7

Gelatinous	88	25 (20)	61 (77)	36	Pyrosomatidae [3] (36, 12)
					Pyrosoma atlanticum (14, 5)
Squids	91	44 (30)	66 (120)	76	*Abraliopsis* sp. [1] (22, 1)
					Pterygioteuthis microlampas (19, 1)
Jellyfishes	54	24 (20)	7 (11)	21	Bougainvilliidae [3] (20, 0.3)
					Alatina sp. [1] (11, 0.1)
Shelled pteropods	68	5 (3)	2 (2)	30	*Clio* sp. [1] (45, 0.2)
					Cavolinia sp. [1] (15, 0.1)
Siphonophores with pneumatophore	9	NA	3 (3)	3	Physonectae [4] (47, 0.2)
					Agalmatidae [3] (47, 0.2)

205

1.3 Forward scattering models

207   In order to compare echosounder backscatter and trawl density (ρ_T), target strength (TS, in dB

208 re 1 m²) scattering models were applied to the trawl's biological samples to calculate the theoretical

209 response of the specimen. A mean backscattering volume $S_{v\,mod}(f)$ was determined for each trawl by

210 making an incoherent weighted summation of the contributions from all acoustic categories in the

211 linear domain (Foote, 1983; Stanton et al., 2012), where the organisms' density served as the weighting

212 factors (Figure 3). All categories are associated to a scattering model with taxa-specific input

213 parameters, applied on the frequency interval 1-200kHz.

214 **Gas-bearing organisms.** The acoustic categories of *fish with swimbladders* and *siphonophore with*

215 *pneumatophore* are organisms bearing a gas-filled inclusion surrounded by a weakly scattering fluid-

216 like body. For fish with a swimbladder, the volume of the fish body (V_f) was approximated as a prolate

217 spheroid with the measured fish length (L_f) as the major axis and L_f/α_f as the minor axis. The fish

218 aspect ratio (α_f) is equal to 5. The swimbladder size was calculated with the equivalent spherical radius

219 $a_{esr} = (\frac{3p_{swb}V_f}{4\pi})^{1/3}$, where p_{swb} was the percentage of V_f used for the swimbladder (Proud et al.,

220 2019). The value p_{swb}=2.5% as reported in Blanluet et al. (2019) was used. The swimbladder

221 backscatter was described using a hybrid scattering model. For lower frequencies ($ka_{esr} \leq 0.2$, ,

222 where k was the wave number in m⁻¹), backscatter was computed using a resonance-scattering model

223 from Scoulding et al. (2015, 2022). This model takes into account the increased backscattering

224 response resulting from the elongation of the swimbladder into a prolate spheroid as defined in Ye

225 (1997) along with a directivity term relative to the incident sound wave and the fish's tilt angle (θ in

226 radians). At broadside incidence ($\theta = \pi/2$), the directivity term was equal to one. The prolate spheroid

227 elongation was defined by a length-to-width aspect ratio (b/a) of 1.5, with *a* and *b* the semi-major and

228 semi-minor axis, respectively. For higher frequencies ($ka_{esr} > 0.2$), the geometrical scattering effect

229 of the swimbladder was modelled using the exact modal series solution for a fluid sphere of equivalent

230 radius a_{esr} defined in Anderson (1950). The transition frequency between the models was chosen at

231 the beginning of the elbow above the resonance frequency (approximately at $ka_{esr} = 0.2$).

232   In the case of siphonophores, the mean equivalent radius a_{esr} of pneumatophore (filled with

233   carbon monoxide gas: g = 0.0012 and h = 0.22 from Benfield et al. (2003) and Lavery et al. (2007)) was

234   fixed at 0.5 mm, based on Benfield et al. (2003), Kloser et al. (2016) and Proud et al. (2019). The

235   scattering from the fish body and the nectophores (fluid-like parts of the siphonophore) were

236   considered to be neglectable (Scoulding et al., 2015). The specific shape and physical model

237   parameters for both categories are summarized in Table 3.

238   **Elastic shell organisms.** The *shelled pteropods* acoustic category was similar to a fluid-like sphere

239   surrounded by a solid shell. It was modelled with a simple high-pass dense fluid model based on Lavery

240   et al. (2007), with a reflection coefficient R=0.5 (Blanluet et al., 2019). The equivalent spherical radius

241   a_{esr} (in m) was estimated as half the length of the measured diameter.

242   **Fluid-like organisms.** All the remaining acoustics categories, including *amphipods, euphausiids and*

243   *decapods*, *gelatinous*, *jellyfish*, *squid* and *fish without swimbladder* were modelled using a model based

244   on the Distorted-Wave Born Approximation (DWBA) scattering model averaged over a normal

245   distribution of orientation angles (Stanton et al., 1998; Stanton and Chu, 2000). The fluid-like

246   organisms were simplified as uniformly-bent and tapered cylinders, except for jellyfish approximated

247   as two prolate spheroidal surfaces (Warren and Smith, 2007) and integrated over 300 integration

248   points along the body axis of total length (L). The length L was defined as the total length for

249   *amphipods*, *euphausiids and decapods* (equivalent to Standard Length 1 in Mauchline, 1981) and

250   *gelatinous*, the mantle length for *squid*, the standard length for *fish without swimbladder* and the bell

251   diameter for *jellyfish*. The cylindrical cross-section radius a (in m) of the organisms was estimated with

252   the ratio L/a summarized in Table 4. The parameters and shape of the scattering model for each

253   category is shown Table 4. Most of the parameters are extracted from Lawson et al. (2004).

254   **Table 3.** Swimbladder and pneumatophore hybrid scattering model parameters.

Parameter	Symbol	Value for swimbladder	Value for pneumatophore	Unit
Heat ratio of gas inclusion	γ_{swb}	1.4 [a]	1.4 [a]	-
Organisms' tissue density	ρ_f	1050 [b]	1030 [c]	kg m^{-3}
Density of air	ρ_a	1.3 [b]	1.3 [b]	kg m^{-3}
Water density	ρ_w	Varying with depth [d]	Varying with depth [d]	kg m^{-3}
Sound speed	c_w	Varying with depth [e]	Varying with depth [e]	m s^{-1}
Thermal conductivity of air	k_a	5.5×10^{-3} [b]	5.5×10^{-3} [b]	cal m^{-1} s^{-1} °C^{-1}
Length/width ratio	b/a	1.5 [f]	2.35 [f]	-
Shear modulus	μ_r	5.10^5 [g]	5.10^5 [h]	N m^{-2}
Dynamic viscosity	ξ	1 [g]	4/3 [i]	kg m^{-1} s^{-1}
Surface tension	s	200 [b,g]	0.074 [i]	N m^{-1}
Heat capacity of air	c_{pa}	240 [b]	240 [b]	cal kg^{-1} °C^{-1}
Sound speed contrast	h	0.22 [j]	0.22 [c]	-

9

Density contrast	g	0.0012 [j]	0.0012 [c]	-
Percentage of volume of fish occupied by the swimbladder	p_{swb}	2.5 [f]	NA	%
Tilt angle	θ	0 [g]	25 [k]	°

a. Kloser et al., 2002,
b. Love, 1978,
c. Lavery et al., 2007,
d. Estimated with the closest CTD profiles
e. Calculated with the equation from Mackenzie, 1981,
f. Blanluet et al., 2019,
g. Scoulding et al., 2015,
h. Empirically chosen identical as swimbladder because we had no value available,
i. Proud et al., 2017,
j. Jech et al., 2015,
k. Empirically chosen for the pneumatophore.

Table 4. Weak scatterers models parameters for each acoustic category. Radius of curvature ρ_c/L were chosen empirically, where $\rho_c/L \rightarrow \infty$ defines a straight cylinder shape. N defines the Normal distribution.

Organism (Scattering model)	Length-to-cylindrical radius (L/a)	Orientation (Mean, STD)	Density contrast (g)	Sound speed contrast (h)	Radius of curvature (ρ_c/L)
Fishes without Swimbladder (DWBA *uniformly-bent cylinder***)**	8 [a]	N(0,30) [a]	1.010 [a]	1.025 [a]	10
Amphipods (DWBA *uniformly-bent cylinder***)**	3 [c]	N(0,30) [c]	1.058 [b]	1.058 [b]	6
Euphausiids, Decapods<25mm (DWBA *uniformly-bent cylinder***)**	10.5 [b]	N(20,20) [b]	1.016 [b]	1.019 [b]	3
Euphausiids, Decapods>25mm (DWBA *uniformly-bent cylinder***)**	10.5 [b]	N(20,20) [b]	$5.485 \times L \times 10^{-4} + 1.002$ [b]	$5.942 \times L \times 10^{-4} + 1.004$ [b]	3
Gelatinous (DWBA *uniformly-bent cylinder***)**	4 [c]	N(0,30) [c]	1.003 [b]	1.003 [b]	10
Shelled pteropods (*High-pass fluid sphere***)**	NA	NA	R=0.5=(gh-1)/(gh+1) [a,b]	NA	NA
Squids (DWBA *uniformly-bent cylinder***)**	5 [d]	N(0,20) [d]	1.029 [d]	1.041 [d]	10
Jellyfishes (*DWBA two prolate spheroidal surfaces***)**	NA	NA	1.02 [a]	1.02 [a]	NA

a. Blanluet et al., 2019,
b. Lawson et al., 2004,
c. Lavery et al., 2007,
d. Jones et al., 2009.

1.3.1 Prediction of modelled backscattering strength with forward approach

The modelled volume backscattering strength $S_{v,mod}$ was estimated for each trawl as:

$$S_{v,mod}(f) = 10log_{10}\left(\sum_{i=1}^{N_{taxa}} \rho_{T,i}\, \sigma_{bs,i}\right) \qquad (1)$$

278   with N_{taxa} the number of taxa groups, $\rho_{T,i}$ the density in individual (N ind./$V_{sampled}$ in m^{-3}) and $\sigma_{bs,i}$ the

279   backscattering cross-section of each taxa group i, defined as:

$$\sigma_{bs,i} = \sum_{j=1}^{n_{length\ class}} D_j^i\, \sigma_{bs}{}_j^i \qquad (2)$$

280   For each taxa group i, $\sigma_{bs}{}_j^i$ was the modelled backscatter cross-section (in m²) of length class j. D_j^i was

281   the proportion of individuals of length class j in the taxa group i. $S_{v,mod}(f)$ was the total theoretical

282   backscattering response over frequency f and was determined for each trawl.

1.3.2 Uncertainty analysis

284   Model parameters for the scattering models were derived from literature. However, the

285   variability in parameters across a wide range of taxa introduced a source of uncertainty. To assess the

286   reliability of model predictions, 1000 simulations for each size were performed, randomly selecting

287   input values from uniform distributions derived from maxima in literature when available or centred

288   around the reference value (Supplementary Table S3). Uniform distributions were selected to cover

289   the entire spectrum of variability in model parameters and their influence on the simulated backscatter

290   (Proud et al., 2019). The uncertainty around scattering predictions was defined as the standard

291   deviation of the simulation results over the total modelled backscatter. For the fluid-like models

292   (DWBA), the parameters of density and sound speed contrast g and h and the aspect ratio L/a were

293   evaluated. As for the resonant-scattering model, the parameters considered were α_f, p_{swb}, b/a and

294   θ. The impact of the other parameters of the resonant model were considered neglectable compared

295   to those involved in the definition of the size and shape of the gas-filled inclusion. The length of

296   organisms was not included in the uncertainty analysis as it was measured on all organisms from net

297   samples. The incertitude on the orientation, relative to the direction of incidence, was simulated with

298   a normal distribution of angle in the DWBA model.

**1.4 Comparison of *in situ* and modelled acoustics**

300   This study gathered campaigns conducted over a 10 year-period with minimal variations in the

301   sampling protocols. Notably, trawling depth was chosen depending on the scattering layers detected

302   by the echosounder to study all types of scattering layers in most sea-experiments. Yet the most recent

303   survey WARMALIS-1 applied a different sampling strategy where trawling was performed

304   systematically from the surface down to 200m (oblique tow) and at 500m (horizontal tow) for each

305   station. Whenever the quality of echosounder data was not sufficient to calculate $S_{v,obs}$ (mainly due

11

306   to bad weather and a strong swell creating empty pings) the corresponding trawl was excluded from

307   the dataset. The final dataset contained 75% of the original trawls (n=144) at 38kHz and 59% (n=112)

308   at 70kHz.

309   The difference of volume backscattering strength $\Delta S_{v,f}$ between $S_{v,mod}(f)$ and $S_{v,obs}(f)$ was

310   calculated as:

$$\Delta S_{v,f} = S_{v,obs}(f) - S_{v,mod}(f) \tag{3}$$

311   with $\Delta S_{v,f}$ calculated at f=38 kHz and f=70 kHz, allowing us to measure the difference between the two

312   acoustic densities: observed and modelled from trawl. To explore the link between $\Delta S_{v,38}$ and $\Delta S_{v,70}$,

313   a linear regression (lm) was fit to the data using R statistical software (R Core Team, 2023).

314
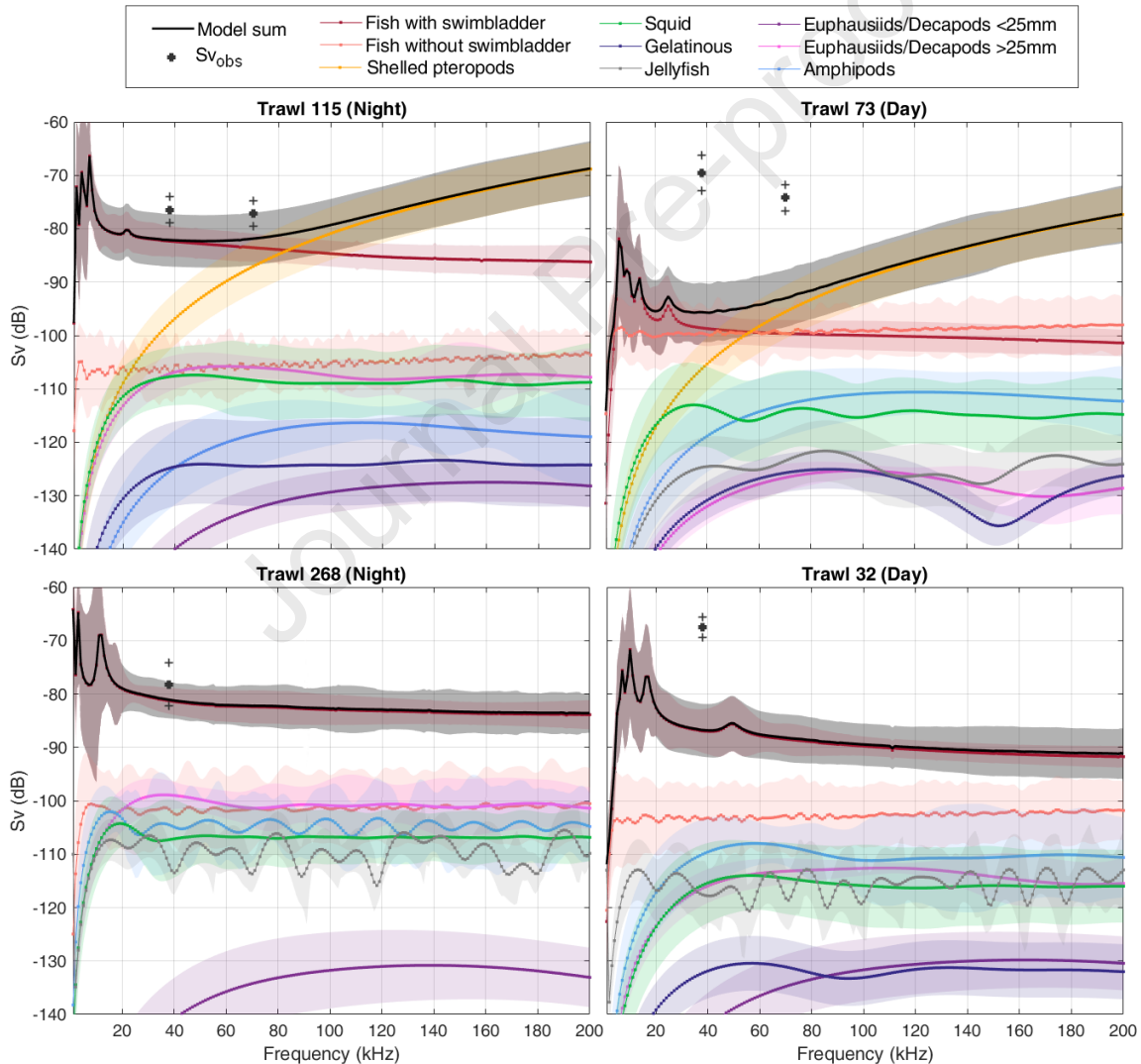
Figure 3. Forward modelling results for each category compared to the observed $S_{v,EK60}$ for four
trawls: #115 (NEC5, d_{trawl}=169m), #268 (WARM, d_{trawl}=545m), #73 (NEC3, d_{trawl}=72m) and #32 (NEC2,
d_{trawl}=509m). The modelled backscattering response $S_v(f)$ in dB re 1 m^{-1} of each acoustic category
caught in the trawls are in coloured solid lines. The total modelled response $S_{v,mod}(f)$ summing the

12

319 contribution of all taxa is in solid black line. Shaded areas are the standard deviations of backscattering

320 responses. In trawls #268 and #32, there is a partial overlap between the contribution of fish with

321 swimbladders (red line) and $S_{v,mod}(f)$ (black line), and the response of fish with swimbladders is

322 scarcely discernible. The *in situ* acoustic densities $S_{v,EK60}$ in *dB re 1 m⁻¹* at 38 kHz and 70kHz are

323 denoted by a black thick cross with their standard deviation in thin crosses. $S_{v,EK60}$ at 70kHz is only

324 available for trawls at depths shallower than 400m.

1.4.1 Generalized Linear Model (GLM)

326 Generalized linear regression models (GLM) with Gaussian (identity-link) form were used to

327 explore how $\Delta S_{v,f}$ was associated with the composition of trawls and the sampling characteristics. The

328 predictor variables used in the GLM were: density of fish with swimbladders (ρ_{SWB}), density of

329 crustaceans (sum of density of amphipod and euphausiid combined as ρ_{crust}), gelatinous density (sum

330 of density of gelatinous and jellyfish as ρ_{gelat}), trawling depth (d_{trawl}) and relative weight of fish with

331 swimbladders, crustaceans and gelatinous. The relative weights represented the measured weight of

332 a taxa group (in g) over the total weight of the trawl. No collinearity among predictors was detected.

333 After examining the distribution of densities, they were transformed into logarithmic scale, $\log10(\rho)$,

334 to better fit the residuals to a Normal distribution. The analysis was performed separately for 38 and

335 70kHz, and for day and night trawls (51 trawls for day and 93 at night) to better account for the impact

336 of DVM (Casey and Myers, 1998). The best models were selected with the compensated Akaike

337 Information Criteria (AICc; R package Mazerolle, 2023). The 4 optimal models (two for each frequency

338 at both day and night-period) are presented in this study. Analyses were performed with R statistical

339 software (R Core Team, 2023), version 4.3.1. Marginal effect plots showing the predicted $\Delta S_{v,f}$ for the

340 significant variables (p-value<0.05) from the GLM models were plotted with the 'ggeffects' package

341 (Lüdecke, 2018, version 1.2.2). The pseudo R-squared (R²) of the models were determined with the

342 McFadden (1973) metric.

2. Results

2.1 Biological sampling

345 Trawl sampling gathered a total number of 98,896 specimens, which represent a combination

346 of different taxonomic levels including 306 species, 311 genus, 186 families and 55 orders (Table 2).

347 The higher number of genera compared to species was a result of the inability to identify all specimen

348 species due to their conservation state. Only 55% of the total specimens were determined at the

349 species level, 8% at the genus level only, 30% at the family level, and 5% at the order level. Among the

350 specimens that could not be identified at the species level, 58% were gelatinous organisms.

351   Myctophidae, Sternoptychidae and Gonostomatidae were the main fish families sampled.

352   *Ceratoscopelus warmingii* was the most abundant species caught for fish with swimbladders. Fishes

353   without swimbladder were mainly represented by Bathymyrinae subfamily (leptocephalus larval stage)

354   and *Lobianchia gemellarii*. *Diaphus perspicillatus* presenting a gas-filled inclusion at the juvenile stage

355   only was the most abundant species classified in both fish with or without swimbladder. Decapods and

356   Euphausiids were mainly represented by *Thysanopoda* sp., *Euphausia mucronata* and *Janicella*

357   *spinicauda*. Various species of the Phronimidae family, particularly *Phronima sedentaria*, and of the

358   Phrosinidae family, including *Phrosina semilunata*, were collected within the amphipods taxa.

359   Cephalopod specimens included *Pterygioteuthis* and *Abralia* genus. The family Bougainvilliidae

360   represented most of the recognisable jellyfish samples while the gelatinous category contained

361   predominantly *Pyrosoma* sp. and Salpidae. Families Agalmatidae and Physonectae represented most

362   of the siphonophores with pneumatophores. Many gelatinous organisms caught in trawls were not

363   sufficiently well preserved to accurately estimate their morphology and identify their species.

364   **2.2 Forward approach $S_{v,mod}(f)$**

365   When varying the input parameter values (Supplementary S3), the standard deviation of

366    $S_{v,mod}(f)$ was +/- 5dB in average at 38 and 70 kHz (Figure 3). The resonance scattering region of gas-

367   bearing organisms situated between 1 and 30 kHz exhibited the highest variability (+/- 10dB in

368   average). The modelled results indicated that scatterers with fluid-like properties had a negligible

369   impact on $S_{v,mod}$, which was dominated by the response of fish with swimbladders in the majority of

370   trawls (Figure 3). When caught in trawls, elastic-shelled pteropods were the strongest scatterers at

371   frequencies > 50-70kHz. In rare cases, some fluid-like categories had a density and a size distribution

372   that led to a scattering response equal or higher than fish with swimbladders at f > 50kHz (e.g. Figure

373   3, Trawl 73). The response of the siphonophores with pneumatophore, the other gas-bearing

374   organisms' category, did not have a major impact on $S_{v,mod}$.

375   **2.3 Variability of $\Delta S_{v,f}$ across trawls**

376   Across the 144 trawls, $\Delta S_{v,f}$ spanned a range of [-1.5, 42.1] dB at 38 kHz and [0.9, 42.4] dB at

377   70 kHz, with a median of 16 dB for the combined distribution of both frequencies. In trawls where

378   d_{trawl} was less than 400m (within the maximum emission range of 70 kHz), $\Delta S_{v,38}$ and $\Delta S_{v,70}$ followed

379   a linear regression (Figure 4a) with a slope of 0.96 (associated with a standard error of 0.03). This

380   suggested that the variability of $\Delta S_{v,f}$ was consistent for both frequencies. $\Delta S_{v,f}$ was >0 (Figure 4b),

381   indicating that the modelled volume backscatter $S_{v,mod}$ derived from trawl catch was lower than the

382   observed $S_{v,obs}$ from the echosounder. Only two trawls, situated in the mesopelagic layer with

383   d_{trawl}>200m, exhibited a $\Delta S_{v,38}$<0. On average, $\Delta S_{v,f}$ was higher during daytime trawls compared to

14

384   night-time trawls for both frequencies, with median values of 19 dB and 22 dB for $\Delta S_{v38,day}$ and

385      $\Delta S_{v70,day}$, and a median of 14 dB for $\Delta S_{v38,night}$ and $\Delta S_{v70,night}$ (Figure 4b).
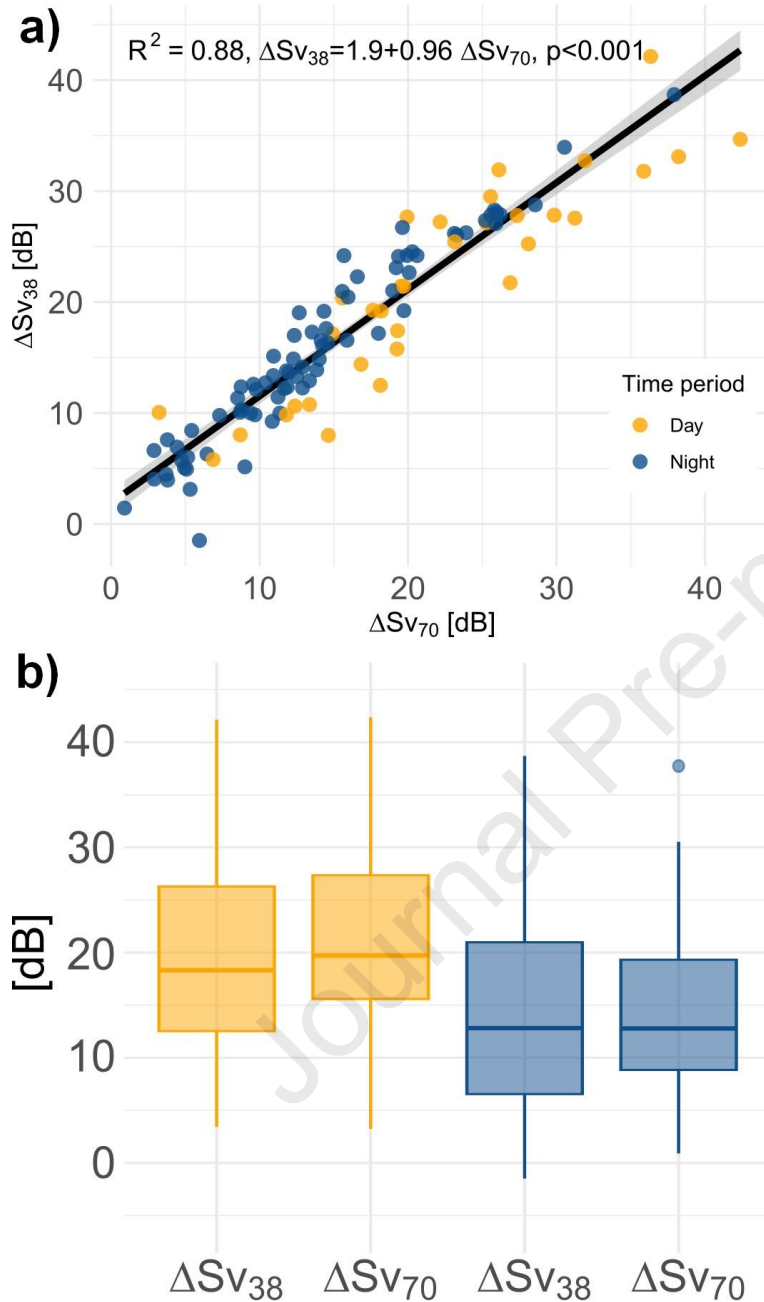
386

387   **Figure 4.** Description of $\Delta S_{v,f}$ in relation with time-period. (a) Relationship between ΔS_{v38} and ΔS_{v70}

388   for each trawl with a linear regression fit (lm) in solid black line and the associated metrics (R², p-value

389   and regression equation). Shaded areas represent 95% confidence interval. Dots represent each trawl

390   with day in yellow and night in blue. (b) Summarized $\Delta S_{v,f}$ for day (yellow) and night (blue) trawls at

391   38 kHz (ΔS_{v38}) and 70 kHz (ΔS_{v70}). Horizontal line within each box is the median value, box limits are

392   the inter-quartile range, i.e. 25 and 75% quantiles. The whiskers (vertical lines) are 1.5 times the inter-

393   quartile range. Dots represent potential outliers.

2.4 Effect of organisms' density

The final models are displayed in Table 5, with only a single model for each day/night and frequency combination because the level of uncertainty in model structure was minimal (i.e., all other subsequent models had dAIC > 2, as shown in Supplementary Table S4). Out of all the predictors examined in the GLM, the log density of fish with swimbladders captured in trawls ($log10(\rho_{SWB})$), and the relative weight of fish with swimbladders (% weight fish SWB) were included in all four models selected with AICc, for both day and night trawls at 38 and 70kHz (Table 5). The predictor $log10(\rho_{SWB})$ was associated with a negative coefficient (Table 5), indicating that $\Delta S_{v,f}$ decreased in trawls with a high density of fish with swimbladders (Figure 5). $\Delta S_{v,f}$ also decreased with % weight fish SWB, in trawls where a large proportion of the sampled weight was represented by fish with swimbladders (Figure 5 and Table 5). Finally, the density of crustaceans, $log10(\rho_{crust})$, was included in the day-time GLM for $\Delta S_{v,70}$, with a negative coefficient indicating a decrease of $\Delta S_{v,70}$ in day-time trawls with a larger density of crustaceans at 70kHz.

2.5 Effect of trawling depth

The depth of trawls (d_{trawl}) was included in night-time models selected with AICc (Table 5). $\Delta S_{v,f}$ decreased in deeper trawls (Figure 5). The selected models explained around 80% of the variance of $\Delta S_{v,f}$ during the night and between 60 to 70% for day-time (Table 5). This finding highlighted that the models did not explain day-time discrepancies between trawl and acoustic observations to the same extent as they did in night-time scattering layers. The other predictors tested were not included in the selected GLM (Supplementary Table S4).

Focusing on the impact of depth, the distribution of $\Delta S_{v,f}$ was studied in two depth layers as in Figure 6: epipelagic ($d_{trawl} \leq 200m$) and mesopelagic ($[200, 800]m$ for 38 kHz and $[200, 400]$ for 70kHz) layers. $\Delta S_{v,f}$ was lower in the mesopelagic layer for both frequencies with a minimum at night (median $\Delta S_{v,f}$ of 3.9 and 5.0 dB, for 38 and 70 kHz, respectively), at the exception of day-time 70kHz. 90% of $\Delta S_{v,38} \leq 5dB$ (15 trawls) were located in the night-time mesopelagic layer, which is the scattering layer with the least average difference between $S_{v,mod}$ and $S_{v,obs}$ (Figure 4).

Table 5. GLM's results for the 4 final models (rows) selected based on the lowest AICc (see Table S3 for full model selection outputs). The response variables ΔS_{v38} and ΔS_{v70} are modelled separately and are split into day/night trawls. The proportion of variance explained (R^2), the beta-coefficients from the GLM of the predictor variables in each model and their standard errors (STD) are indicated for each model. Predictor variables are depth (d_{trawl}), density of fish with swimbladders in logarithmic scale ($log10(\rho_{SWB})$), relative weight of fish with swimbladders (% weight fish SWB) and density of

426   crustaceans in logarithmic scale ($\log10(\rho_{\text{crust}})$). Blank cases indicate the variables not included in the

427   GLM selected with AICc criteria. All predictors are associated to a p-value<0.05.

$\Delta S_{v,f}$ (kHz)	Period	R^2	$\log10(\rho_{\text{Fish SWB}})$ (STD)	% weight fish SWB (STD)	d_{trawl} (STD)	$\log10(\rho_{\text{crust}})$ (STD)
38	Day	62%	-6 (1)	-9 (5)		
70	Day	73%	-6 (1)	-15 (6)		-4 (2)
38	Night	80%	-6 (1)	-8 (2)	-0.03 (0.007)	
70	Night	78%	-6 (1)	-6 (2)	-0.04 (0.007)	

428
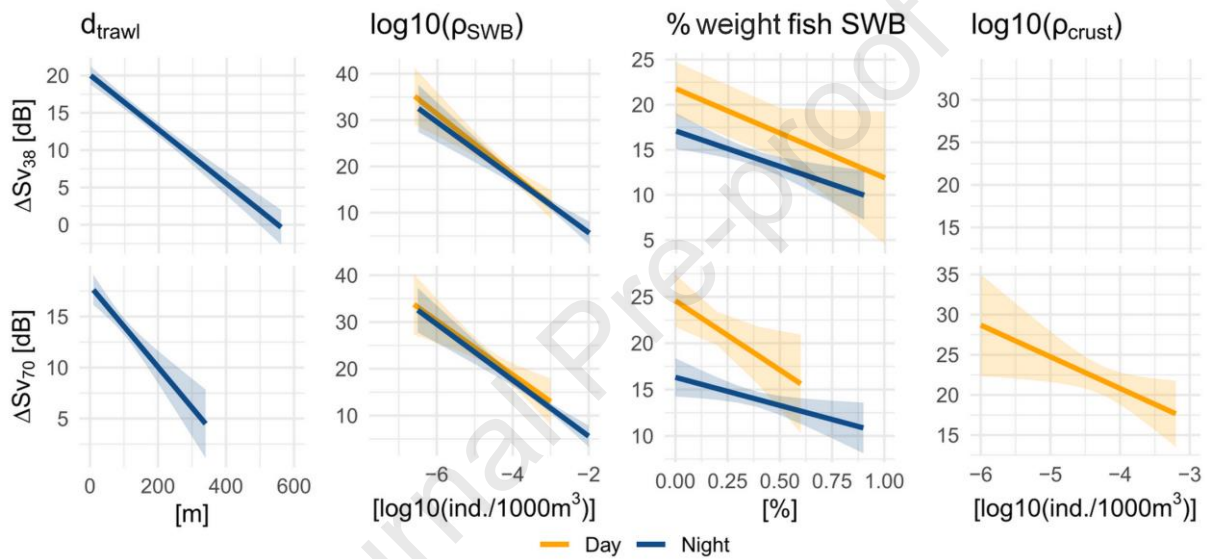
429

430   **Figure 5.** Predicted marginal effects of $\Delta S_{v,f}$ for the 4 GLM models as a function of predictors. $\Delta S_{v,38}$

431   (top) and $\Delta S_{v,70}$ (bottom) predicted for day (yellow solid line) and night (blue solid line) models for the

432   variables d_{trawl}, $\log10(\rho_{\text{SWB}})$, % weight fish SWB and $\log10(\rho_{\text{crust}})$. Shaded areas represent 95%

433   confidence interval of marginal effects. Only the variables selected in the 4 GLM models and presented

434   in Table 5 are plotted. They are all associated to a p-value<0.05.

435
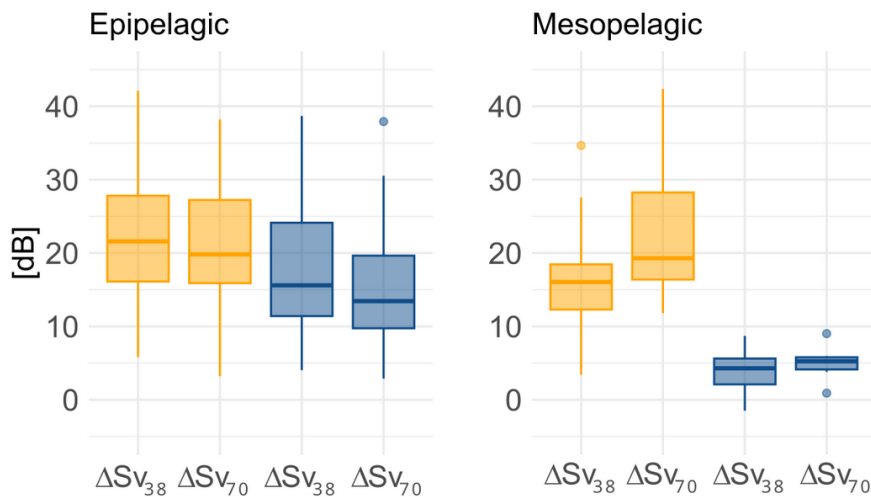
Figure 6. Description of $\Delta S_{v,f}$ distributions per depth layers and time-period: $\Delta S_{v,f}$ in the epipelagic layer (left, $d_{trawl} \leq 200m$) and in the mesopelagic layer (right, $d_{trawl} > 200m$) at 38 kHz (ΔS_{v38}) and 70 kHz (ΔS_{v70}) for day (yellow) and night (blue) trawls. Horizontal line within each box is the median value, box limits are the inter-quartile range, i.e. 25 and 75% quantiles. The whiskers (vertical lines) are 1.5 times the inter-quartile range. Dots represent potential outliers.

441

3. Discussion

Using 144 trawls between the surface and 600m depth, along with 38 and 70 kHz acoustics covering a 10-years period in West tropical Pacific, this study provides information on how acoustic-trawl estimates vary in tropical ecosystems characterized by high biodiversity. The backscattering difference $\Delta S_{v,f}$ between the observed and the predicted acoustic signal using forward modelling was function of the time period (day/night) and decreased with larger weight ratio and density of fish with swimbladders at 38 and 70kHz. In addition, $\Delta S_{v,70}$ during day-time also decreased with the increasing density of crustaceans. The towing depth of each trawl had an effect on $\Delta S_{v,f}$ during the night, with a significantly smaller difference in mesopelagic than epipelagic trawls. These observations show that the interpretation of acoustic-trawl survey results depends on spatial and temporal patterns and is therefore sensitive to the choice of sampling depth and survey time-period (day/night). The values of $\Delta S_{v,f}$ were positive over the entire dataset showing a modelled S_v lower than observed with echosounder value. This consistent positive bias may be linked to an overestimation with hull-mounted echosounders and/or an underestimation of volume backscattering in forward modelling, either due to the models parameterisation or biases in the species diversity and abundance sampled with the trawl (Mair et al., 2005; Blanluet et al., 2019).

3.1 Uncertainties due to acoustics

18

459   The predicted acoustic signal $S_{v,mod}$ depends on the model parameter values and the species
460   composition (diversity and relative abundances) observed in the trawl samples. The incoherent
461   summation of organism contributions relies on the assumption that the backscatter of individual
462   organisms is not affected by neighboring ones, and that their distribution is random within the
463   observed volume. The low densities observed in this study and the mixed nature of the scattering
464   layers allowed us to make this assumption. However, this commonly accepted approach remains
465   simplified and may introduce significant uncertainty into $S_{v,mod}$. The model parameters were chosen
466   from the literature, but were not specific to the tropical Pacific area nor to all taxa caught in trawls,
467   which introduced another source of uncertainty (Lawson et al., 2004, Lucca et al., 2021). $S_{v,mod}$
468   modelled with the parameters chosen in this study was defined as the reference value for all analysis.
469   However, the selection of input parameters for the backscattering models of each taxon group (Table
470   3 and 4) introduced variability in the modelled backscattering response. Model uncertainty analysis
471   indicated that the total volume backscatter could vary within +/-5dB around the reference value of
472    $S_{v,mod}$ at 38 and 70 kHz, solely as a function of input parameters (Figure 3). In trawls where $\Delta S_{v,f} \leq$
473   5dB, predominantly located in the night-time mesopelagic layer, the variability in total modelled
474   backscatter could solely account for the disparity between $S_{v,mod}$ and $S_{v,obs}$. For all other cases, where
475   the median $\Delta S_{v,f}$ was larger than 5 dB, the uncertainty associated with model parameters alone could
476   not explain these differences.

477   As expected, at 38 and 70kHz, $S_{v,mod}$ was primarily dominated by the response of fish with
478   swimbladders, making this group essential for modelling the trawl's backscatter (McClatchie et al.,
479   2000; Kloser et al., 2009; Davison et al., 2015). Among all the parameters for this gas-bearing scattering
480   group, the parameters controlling the swimbladder volume and shape, which vary significantly
481   between species, generated the highest sensitivity on the modelled volume backscatter, as also shown
482   in Proud et al. (2019). Yet assess these parameters for all specimens often require dissection and X-ray
483   or CT-scan to evaluate their variability within species and establish a relation with fish length (Yasuma
484   et al., 2010). These methods are performed only on undamaged specimens with preferably intact
485   swimbladders. However, when bringing mesopelagic fish to the surface, the swimbladder experiences
486   a rapid pressure change during ascent, raising uncertainties regarding whether its morphology and
487   volume remain identical to those in deep layers (Sobradillo et al., 2019; Peña et al., 2023; Sarmiento-
488   Lezcano et al., 2023). For all these reasons, many taxa do not yet have a description regarding the
489   presence of a swimbladder. Choosing to assign them a swimbladder characteristic identical to that of
490   specimens from the same family, to avoid excluding them from the study, introduces a source of error
491   in the modelling (Dornan et al., 2019; Marohn et al., 2021).

492   The group of elastic-shelled pteropods can occasionally dominate the volume backscatter at

493   70 kHz frequency. Their solid shells tend to produce a strong backscattering response even at low

494   densities when compared to fluid-like animals (Stanton et al., 1994). This strong response was

495   computed by a high-pass dense fluid-sphere with an empirical reflection coefficient from Stanton,

496   (1994) which is often used in studies (Lawson et al., 2004; Lavery et al., 2007; Blanluet et al., 2019).

497   This model is relatively simple and does not represent shelled-pteropods that exhibit more complex

498   shapes (spirals or pyramidal shell as *Clio pyramidata* and an opercular opening) and various materials

499   (aragonite, calcite or silica). This assumption might overestimate the actual backscatter. Better

500   knowledge is also required on the scattering responses of gelatinous organisms such as salps and

501   pyrosomes and more broadly of a large range of more rare species (Warren and Smith, 2007; Henschke

502   et al., 2016).

503   During the day, the 70 kHz signal was more sensitive to the density of crustaceans as $\Delta S_{v,70}$

504   decreased with larger densities. Recording acoustic data at higher frequencies (120 and 200 kHz) would

505   help to estimate the effect of the groups of crustaceans and fluid-like organisms (gelatinous, squids

506   and jellyfishes) in the upper layer as suggested in other studies (e.g., Jech et al., 2018; Lucca et al.,

507   2021) as they are further away from the resonance frequencies of gas-filled structures often situated

508   between 18 and 70 kHz. At these higher frequencies, the relationship between volume backscatter

509   and biomass becomes more linear as proposed in Benoit-Bird, (2009). However, the data at 120 and

510   200 kHz in our surveys were of bad quality. Therefore, our findings likely depict trends related to gas-

511   bearing mesopelagic fishes.

512   **3.2 Micronekton trawl sampling**

513   The large $\Delta S_{v,f}$ can also be linked to the underestimation of abundance and biases in the

514   species composition as caught by the trawl sampling. Utilizing forward modelling on biological

515   sampling necessitates precise estimates of the abundance, weight, size distribution, and morphological

516   characteristics of the groups of species defined in the model to accurately calculate the theoretical

517   mean volume backscatter in a specific sampled layer. However, the tropical Pacific Ocean has a very

518   high species diversity with potentially strong spatial heterogeneity in the horizontal and vertical

519   distributions of species, making it difficult to achieve comprehensive trawl sampling.

520   Trawl catchability is a function of its design and operational features (i.e., length, mesh size,

521   trawl opening and towing speed) and the characteristics of the organisms captured (i.e., swimming

522   speed, length and shape; Grimaldo et al., 2022). Some organisms tend to avoid the trawl or escape it

523   after entering, with their chance of escaping the trawl increasing with the swimming speed (Bethke et

524   al., 1999; De Robertis et al., 2017a; Grimaldo et al., 2022). With trawls towed around 2 to 3 knots (as

525   in this study), fast swimming species in mesopelagic fishes and squids (Peña et al., 2018) can likely

526   escape or stay away from the trawl (Kaartvedt et al., 2012; Davison et al., 2015; Underwood et al.,

527   2020). Increasing the towing speed would potentially reduce the avoidance factor but is not

528   conceivable with all vessels and/or all trawls. The avoidance factor may be more pronounced in the

529   surface layers where organisms might detect the approaching trawl due to sunlight during the day and

530   artificial lights from the vessel during the night (Pakhomov and Yamamura, 2010). Thus, the largest

531   differences of $\Delta S_{v,f}$ in the epipelagic layer might, in part, be attributed to the influence of light leading

532   to lower catchability.

533   In addition, the mesh-size selectivity, is also important in the trawl-based estimates of

534   micronekton biomass. The size selectivity leads to an incomplete length distribution of micronekton

535   specimen (Lawson et al., 2004; Proud et al., 2019). The net in our study presenting a graded mesh, all

536   taxa may not be herded by the largest mesh (80mm) at the entrance nor gathered homogeneously

537   down to the cod-end (Heino et al., 2011; De Robertis et al., 2017a). The smallest and least mobile

538   micronekton organisms, mainly crustaceans, gelatinous and shelled-pteropods, may pass through the

539   largest mesh to be captured only in the narrowest mesh at the end of the trawl (Kloser et al., 2009).

540   This selectivity would affect the determination of the effective opening surface utilized to estimate the

541   sampling volume and introduce a correlation with the size distribution of organisms. The replication of

542   tows at one station for the same scattering layer would reduce the variability in length distribution and

543   help assess the size selectivity (Lawson et al., 2004).

544   Underestimation of mesopelagic fish cannot explain alone the variability of $\Delta S_{v,f}$. Large

545   differences ($\Delta S_{v,f}$>15 dB) were observed in all depth layers and time-period at the exception of night-

546   time mesopelagic layer. They were not systematically associated with a low density of fish with

547   swimbladders (relatively compared to the other micronektonic densities). In those cases, ρ_{SWB} alone

548   could not explain the variability of $\Delta S_{v,f}$ indicating that i) acoustic backscatter was due to other species

549   not sampled by the trawl (i.e. possibly siphonophores with pneumatophores), and/or ii) the acoustic

550   theoretical response of the present specimens was not properly modelled. Gelatinous organisms in

551   particular are sensitive to both aspects, because they are fragile and their acoustic response is poorly

552   known. The trawl used in this study is not well suited to collect jellyfish and gelatinous colonial

553   organisms (salps, siphonophores). Those that end up in the cod-end are often brought aboard broken

554   or damaged, which renders their counting and morphological description difficult. Siphonophores can

555   contribute significantly to the mean volume backscattering strength and generate a signal as strong as

556   mesopelagic fish in total mesopelagic backscatter (Proud et al., 2019) with a consequent impact on

557   biomass estimates (Blanluet et al., 2019, Proud et al., 2019). In this study, siphonophores were caught

558   in few trawls (only 3%) and their abundance might have been underestimated because of the difficulty

559   to catch fragile colonial organisms in trawls. Their abundance and length remain largely unknown in

560   open ocean (Kloser et al., 2016). Pneumatophores have been reported to a length ranging from 0.05

561 to 1.5 mm (Benfield et al., 2003; Lavery et al., 2007; Kloser et al., 2016) and the importance of the

562 contribution of their fluid-like parts (bracts and nectophores) is still debated (Lavery et al., 2007), which

563 makes their inclusion in forward problem complex in the absence of precise observations.

564 Supplementing trawl sampling with nets designed for capturing smaller species and

565 zooplankton, such as the Methot Isaac Kidd and/or the Multinet (Blanluet et al., 2019), could enhance

566 the identification and abundance estimates of gelatinous and other fragile, smaller organisms.

567 Zooplankton and small organisms can form dense aggregations and sometimes contribute to more

568 than 50% of backscattering, as observed at 120kHz with copepods in Lawson et al. (2004). Overall,

569 despite the use of all sampled taxa in this study to take into account the diversity of micronekton

570 organisms, our results are focused on mesopelagic fish with swimbladders abundance estimates.

571 **3.4 Variability of observed scattering layers**

572 The spatial organization of scattering layers plays a role in the variability of $\Delta S_{v,f}$. In our model,

573 scattering layers were considered homogenous all along the tows. However, that this is not necessarily

574 true (Benoit-Bird et al., 2017). Patchy distributions and small schools were often observed on the

575 echosounder data, especially in surface layers. These aggregations have a strong acoustic response but

576 are not homogeneously distributed and may have been missed by our trawl, explaining discrepancies

577 between sampling methods with a strong acoustics observation not found in trawl samples (Lawson

578 et al., 2004). Clustering algorithms seem to make it possible to differentiate sublayers that are

579 inhomogeneous from an acoustic point of view (Blanluet et al., 2019). Taking into account these

580 different strata could help understand which areas have been better sampled by the trawl. This can be

581 achieved by modelling the acoustic response based on micronektonic compositions and comparing it

582 to the signal from different sub-layers, instead of relying on the averaged backscatter of a single large

583 scattering layer.

584 **3.4 Perspectives and complementary sampling methods**

585 To progress in our understanding of the relationships between hull-mounted acoustic data and

586 trawl sampling data, complementary approaches are needed to improve species identification and

587 individual abundance estimates. Optical devices are a promising tool to identify species, measure and

588 count organisms, either independently (Williams et al., 2018; Gastauer et al., 2022) or in conjunction

589 with another measurement method, such as using them on a trawl to document organisms entering

590 the net (Allken et al., 2021) or an acoustic probe (Marouchos et al., 2016). Infrared stereo-camera

591 profiles down to 150m depth in nearshore stations have been used to estimate the sizes and densities

592 of micronekton in scattering layers (Benoit-Bird, 2009). These data showed a correlation between the

593 densities of micronekton (mainly myctophids without gas-swimbladder) and volume scattering from

594 echosounders. However, optical measurements in deep scattering layers require the use of a light

595 source that might affect the behaviour of the organisms. Peña et al. (2020), Geoffroy et al. (2021) and

596 Underwood et al. (2021) highlighted the change in behaviour of organisms to an artificial light source,

597 with clear avoidance of mesopelagic fish in white light. Uncertainty remains about the impact of other

598 colours and the wavelength used, but it could introduce another set of biases to biomass estimates.

599 Acoustic profilers or probes submerged in mesopelagic layers appear to be a possible approach

600 linking trawls and acoustics (Kloser et al., 2016). Given the limited range of emission of hull-mounted

601 sounders at high frequencies, vertical profilers using frequencies higher than 70 kHz would be useful.

602 Wideband acoustic profilers in particular, presenting a high-resolution and a smaller insonified volume

603 than hull-mounted echosounder in deep layers, offer a better chance at detecting individual targets

604 (Bassett et al., 2020; Cotter et al., 2021). Weak, fluid-like scatterers are not masked by gas-filled

605 organisms in the small sampled volume and are therefore detectable with echo-counting algorithms

606 to estimate their density (Agersted et al., 2021a; Cotter et al., 2021). To study scattering layers with

607 trawls and profiler simultaneously, a solution would be to add the wideband profiler on the pelagic

608 trawl opening to record organisms in front of it as in Underwood et al. (2020). This setup detect the

609 behaviour of the organisms in front of the trawl and is a useful tool to calculate the avoidance and

610 escapement rate of a trawl. The question of what organisms are actually detected with the profiler

611 remains when estimating biomass. To accurately compute the total backscatter, it is essential to

612 determine the proportion and exact acoustic response of each taxa across a wide frequency band, as

613 opposed to relying solely on the response at discrete frequencies (Proud et al., 2019). The wideband

614 properties allow us to study the detected targets response as a function of frequency band. Using this

615 information is the next step to better understand the composition of mixed scattering layers by

616 classifying the different target responses as in Verma et al. (2017) and Agersted et al. (2021b) and link

617 them with broad taxa groups. We are currently systematically associating such wideband profiler to

618 sampling trawl to assist in the correction of collected density of organisms when quantifying biomass.

619 Finally, it seems that techniques based on environmental DNA could complement the trawl sampling

620 to obtain key information on species composition and even rough estimate of abundance by taxa

621 (Bessey et al., 2021; Govindarajan et al., 2022, 2023; Albonetti et al., 2023).

622

623 **3.5 Concluding remarks**

624 The comparison of micronekton density in acoustic-trawl surveys has highlighted significant

625 disparities in organism abundance in tropical ecosystems defined by a high biodiversity. It showed the

626 relationship between these differences with depth, time-period and composition of the trawl. Even

627 when including all categories of micronekton scatterers, our acoustic-trawl surveys favoured the

628   estimation of the density of mesopelagic fish; a result common to most mesopelagic studies at 38kHz

629   (Scoulding et al., 2015; Proud et al., 2019; Dornan et al., 2022). In this study, the mesopelagic layer,

630   especially at night, displays the smallest divergence between acoustics and trawl. In this case, it is

631   recommended to initially focus on this layer for estimating mesopelagic biomass. This layer shows the

632   most consistent results between the two methods, making them easier to interpret.

633   Finally, it is obvious that the sampling of micronekton should be conducted concurrently using

634   a combination of methods, including hull-mounted echosounders, towed probes employing acoustics

635   and optics, alongside trawl samplings and genomics. Validating acoustic measurements with other

636   methods would help understanding and reducing the large differences between acoustics and trawl

637   sampling to improve abundance and biomass estimates of micronekton in tropical pelagic ecosystems.

652   **Authors contributions**

653   Laure Barbin: Conceptualization, methodology, formal analysis, writing original draft, writing review

654   and editing ; Anne Lebourges-Dhaussy: Conceptualization, writing review and editing ; Valérie Allain:

655   Project administration, writing review and editing ; Aurore Receveur: Conceptualization, writing

656   review and editing, formal analysis ; Patrick Lehodey: Conceptualization, writing review and editing ;

657   Jérémie Habasque : writing review and editing ; Elodie Vourey : Data Curation, Validation ; Annie

658   Portal : Data Curation; Gildas Roudaut : Data Curation ; Christophe Menkes: Conceptualization,

659   Project administration, writing review and editing.

References

Agersted, M.D., Khodabandeloo, B., Klevjer, T.A., García-Seoane, E., Strand, E., Underwood, M.J., Melle, W., 2021a. Mass estimates of individual gas-bearing mesopelagic fish from *in situ* wideband acoustic measurements ground-truthed by biological net sampling. ICES Journal of Marine Science 78, 3658–3673. https://doi.org/10.1093/icesjms/fsab207

Agersted, M.D., Khodabandeloo, B., Liu, Y., Melle, W., Klevjer, T.A., 2021b. Application of an unsupervised clustering algorithm on *in situ* broadband acoustic data to identify different mesopelagic target types. ICES Journal of Marine Science 78, 2907–2921. https://doi.org/10.1093/icesjms/fsab167

Albonetti, L., Maiello, G., Cariani, A., Carpentieri, P., Ferrari, A., Sbrana, A., Shum, P., Talarico, L., Russo, T., Mariani, S., 2023. DNA metabarcoding of trawling bycatch reveals diversity and distribution patterns of sharks and rays in the central Tyrrhenian Sea. ICES Journal of Marine Science 80, 664–674. https://doi.org/10.1093/icesjms/fsad022

Allain, V., Menkes, C., 2018. WALLALIS cruise, Alis R/V. https://doi.org/10.17600/18000523

Allain, V., Menkes, C., 2016. NECTALIS-5 cruise, Alis R/V. https://doi.org/10.17600/16004200

Allain, V., Menkes, C., 2015. NECTALIS-4 cruise, Alis R/V. https://doi.org/10.17600/15004000

Allain, V., Menkes, C., 2014. NECTALIS-3 cruise, Alis R/V. https://doi.org/10.17600/14004900

Allain, V., Menkes, C., 2011a. NECTALIS-1 cruise, Alis R/V. https://doi.org/10.17600/11100050

Allain, V., Menkes, C., 2011b. NECTALIS-2 cruise, Alis R/V. https://doi.org/10.17600/11100070

Allken, V., Rosen, S., Handegard, N.O., Malde, K., 2021. A deep learning-based method to identify and count pelagic and mesopelagic fishes from trawl camera images. ICES Journal of Marine Science 78, 3780–3792. https://doi.org/10.1093/icesjms/fsab227

Anderson, T.R., Martin, A.P., Lampitt, R.S., Trueman, C.N., Henson, S.A., Mayor, D.J., 2019. Quantifying carbon fluxes from primary production to mesopelagic fish using a simple food web model. ICES Journal of Marine Science 76, 690–701. https://doi.org/10.1093/icesjms/fsx234

Anderson, V.C., 1950. Sound scattering from a fluid sphere. The Journal of the Acoustical Society of America 22, 426–431. https://doi.org/10.1121/1.1906621

Ariza, A., Garijo, J.C., Landeira, J.M., Bordes, F., Hernández-León, S., 2015. Migrant biomass and respiratory carbon flux by zooplankton and micronekton in the subtropical northeast Atlantic Ocean (Canary Islands). Progress in Oceanography 134, 330–342. https://doi.org/10.1016/j.pocean.2015.03.003

Ariza, A., Lengaigne, M., Menkes, C., Lebourges-Dhaussy, A., Receveur, A., Gorgues, T., Habasque, J., Gutiérrez, M., Maury, O., Bertrand, A., 2022. Global decline of pelagic fauna in a warmer ocean. Nature Climate Change 12, 928–934. https://doi.org/10.1038/s41558-022-01479-2

Arreguín-Sánchez, F., 1996. Catchability: a key parameter for fish stock assessment. Reviews in Fish Biology and Fisheries volume 6, 22. https://doi.org/10.1007/BF00182344

Bassett, C., Lavery, A.C., Stanton, T.K., Cotter, E.D., 2020. Frequency- and depth-dependent target strength measurements of individual mesopelagic scatterers. The Journal of the Acoustical Society of America 148, EL153–EL158. https://doi.org/10.1121/10.0001745

Benfield, M.C., Lavery, A.C., Wiebe, P.H., Greene, C.H., Stanton, T.K., Copley, N.J., 2003. Distributions of physonect siphonulae in the Gulf of Maine and their potential as important sources of acoustic scattering. Canadian Journal of Fisheries and Aquatic Sciences 60, 14. https://doi.org/10.1139/f03-065

Benoit-Bird, K.J., 2009. The effects of scattering-layer composition, animal size, and numerical density on the frequency response of volume backscatter. ICES Journal of Marine Science 66, 582–593. https://doi.org/10.1093/icesjms/fsp013

Benoit-Bird, K.J., Lawson, G.L., 2016. Ecological insights from pelagic habitats acquired using active acoustic techniques. Annual Review of Marine Science 8, 463–490. https://doi.org/10.1146/annurev-marine-122414-034001

710 Benoit-Bird, K.J., Moline, M.A., Southall, B.L., 2017. Prey in oceanic sound scattering layers organize
711   to get a little help from their friends. Limnology and Oceanography 62, 2788–2798.
712   https://doi.org/10.1002/lno.10606
713 Bertrand, A., Bard, F.-X., Josse, E., 2002. Tuna food habits related to the micronekton distribution in
714   French Polynesia. Marine Biology 140, 1023–1037. https://doi.org/10.1007/s00227-001-
715   0776-3
716 Bessey, C., Neil Jarman, S., Simpson, T., Miller, H., Stewart, T., Kenneth Keesing, J., Berry, O., 2021.
717   Passive eDNA collection enhances aquatic biodiversity analysis. Communications Biology 4,
718   236. https://doi.org/10.1038/s42003-021-01760-8
719 Bethke, E., Arrhenius, F., Cardinale, M., Håkansson, N., 1999. Comparison of the selectivity of three
720   pelagic sampling trawls in a hydroacoustic survey. Fisheries Research 44, 15–23.
721   https://doi.org/10.1016/S0165-7836(99)00054-5
722 Blackburn, M., 1968. Micronekton of the eastern tropical Pacific Ocean: Family composition,
723   distribution, abundance, and relations to tuna. Fisheries Bulletin US 67, 71–115.
724 Blanluet, A., Doray, M., Berger, L., Romagnan, J.-B., Le Bouffant, N., Lehuta, S., Petitgas, P., 2019.
725   Characterization of sound scattering layers in the Bay of Biscay using broadband acoustics,
726   nets and video. PLoS ONE 14, e0223618. https://doi.org/10.1371/journal.pone.0223618
727 Brierley, A.S., 2014. Diel vertical migration. Current Biology 24, R1074–R1076.
728   https://doi.org/10.1016/j.cub.2014.08.054
729 Brodeur, R.D., Seki, M.P., Pakhomov, E.A., Suntsov, A.V., 2004. Micronekton - What are they and why
730   are they important? PICES Press 13, 7–11.
731 Burgos, J.M., Horne, J.K., 2008. Characterization and classification of acoustically detected fish spatial
732   distributions. ICES Journal of Marine Science 65, 1235–1247.
733   https://doi.org/10.1093/icesjms/fsn087
734 Casey, J.M., Myers, R.A., 1998. Diel variation in trawl catchability: is it as clear as day and night?
735   Canadian Journal of Fisheries and Aquatic Sciences 55, 2329–2340.
736 Cotter, E., Bassett, C., Lavery, A., 2021. Comparison of mesopelagic organism abundance estimates
737   using *in situ* target strength measurements and echo-counting techniques. JASA Express
738   Letters 1, 040801. https://doi.org/10.1121/10.0003940
739 Czudaj, S., Koppelmann, R., Möllmann, C., Schaber, M., Fock, H.O., 2021. Community structure of
740   mesopelagic fishes constituting sound scattering layers in the eastern tropical North Atlantic.
741   Journal of Marine Systems 224, 103635. https://doi.org/10.1016/j.jmarsys.2021.103635
742 Davison, P.C., Checkley, D.M., Koslow, J.A., Barlow, J., 2013. Carbon export mediated by mesopelagic
743   fishes in the northeast Pacific Ocean. Progress in Oceanography 116, 14–30.
744   https://doi.org/10.1016/j.pocean.2013.05.013
745 Davison, P.C., Koslow, J.A., Kloser, R.J., 2015. Acoustic biomass estimation of mesopelagic fish:
746   backscattering from individuals, populations, and communities. ICES Journal of Marine
747   Science 72, 1413–1424. https://doi.org/10.1093/icesjms/fsv023
748 De Robertis, A., Taylor, K., Williams, K., Wilson, C.D., 2017a. Species and size selectivity of two
749   midwater trawls used in an acoustic survey of the Alaska Arctic. Deep Sea Research Part II:
750   Topical Studies in Oceanography 135, 40–50. https://doi.org/10.1016/j.dsr2.2015.11.014
751 De Robertis, A., Taylor, K., Wilson, C.D., Farley, E.V., 2017b. Abundance and distribution of Arctic cod
752   (*Boreogadus saida*) and other pelagic fishes over the U.S. Continental Shelf of the Northern
753   Bering and Chukchi Seas. Deep Sea Research Part II: Topical Studies in Oceanography 135,
754   51–65. https://doi.org/10.1016/j.dsr2.2016.03.002
755 Demer, D.A., Berger, L., Bernasconi, M., Bethke, E., Boswell, K.M., Chu, D., Domokos, R., Dunford, A.,
756   Fassler, S., Gauthier, S., Hufnagle, L. T., Jech, J. M., Bouffant, N., Lebourges-Dhaussy, A.,
757   Lurton, X., Macaulay, G. J., Perrot, Y., Ryan, T., Parker-Stetter, S., Stienessen, S., Weber, T.,
758   Williamson, N., 2015. Calibration of acoustic instruments. ICES Cooperative Research Report
759   326, 133. http://dx.doi.org/10.25607/OBP-185

Dornan, T., Fielding, S., Saunders, R.A., Genner, M.J., 2022. Large mesopelagic fish biomass in the Southern Ocean resolved by acoustic properties. Proceedings of the Royal Society B: Biological Sciences 289, 20211781. https://doi.org/10.1098/rspb.2021.1781

Dornan, T., Fielding, S., Saunders, R.A., Genner, M.J., 2019. Swimbladder morphology masks Southern Ocean mesopelagic fish biomass. Proceedings of the Royal Society B: Biological Sciences 286, 20190353. https://doi.org/10.1098/rspb.2019.0353

Escobar-Flores, P.C., Ladroit, Y., O'Driscoll, R.L., 2019. Acoustic assessment of the micronekton community on the Chatham Rise, New Zealand, using a semi-automated approach. Frontiers in Marine Science 6, 507. https://doi.org/10.3389/fmars.2019.00507

Fjeld, K., Tiller, R., Grimaldo, E., Grimsmo, L., Standal, I.-B., 2023. Mesopelagics–New gold rush or castle in the sky? Marine Policy 147, 105359. https://doi.org/10.1016/j.marpol.2022.105359

Foote, K.G., 1983. Linearity of fisheries acoustics, with addition theorems. The Journal of the Acoustical Society of America 73, 1932–1940. https://doi.org/10.1121/1.389583

Foote, K.G., Knudsen, H.P., Vestnes, G., MacLennan, D.N., Simmonds, E.J., 1987. Calibration of acoustic instruments for fish density estimation: A practical guide. ICES Cooperative Research Reports (CRR). https://doi.org/10.17895/ices.pub.8265

Gastauer, S., Nickels, C.F., Ohman, M.D., 2022. Body size- and season-dependent diel vertical migration of mesozooplankton resolved acoustically in the San Diego Trough. Limnology & Oceanography 67, 300–313. https://doi.org/10.1002/lno.11993

Geoffroy, M., Langbehn, T., Priou, P., Varpe, Ø., Johnsen, G., Le Bris, A., Fisher, J.A.D., Daase, M., McKee, D., Cohen, J., Berge, J., 2021. Pelagic organisms avoid white, blue, and red artificial light from scientific instruments. Scientific Reports 11, 14941. https://doi.org/10.1038/s41598-021-94355-6

Gjøsæter, J., Kawaguchi, K., 1980. A review of the world resources of mesopelagic fish. FAO Fisheries Technical Paper.

Govindarajan, A.F., Llopiz, J.K., Caiger, P.E., Jech, J.M., Lavery, A.C., McMonagle, H., Wiebe, P.H., Zhang, W. (Gordon), 2023. Assessing mesopelagic fish diversity and diel vertical migration with environmental DNA. Front. Mar. Sci. 10, 1219993. https://doi.org/10.3389/fmars.2023.1219993

Govindarajan, A.F., McCartin, L., Adams, A., Allan, E., Belani, A., Francolini, R., Fujii, J., Gomez-Ibañez, D., Kukulya, A., Marin, F., Tradd, K., Yoerger, D.R., McDermott, J.M., Herrera, S., 2022. Improved biodiversity detection using a large-volume environmental DNA sampler with in situ filtration and implications for marine eDNA sampling strategies. Deep Sea Research Part I: Oceanographic Research Papers 189, 103871. https://doi.org/10.1016/j.dsr.2022.103871

Grimaldo, E., Herrmann, B., Brčić, J., Cerbule, K., Brinkhof, J., Grimsmo, L., Jacques, N., 2022. Prediction of potential net panel selectivity in mesopelagic trawls. Ocean Engineering 260, 111964. https://doi.org/10.1016/j.oceaneng.2022.111964

Heino, M., Porteiro, F.M., Sutton, T.T., Falkenhaug, T., Godø, O.R., Piatkowski, U., 2011. Catchability of pelagic trawls for sampling deep-living nekton in the mid-North Atlantic. ICES Journal of Marine Science 68, 377–389. https://doi.org/10.1093/icesjms/fsq089

Henschke, N., Everett, J.D., Richardson, A.J., Suthers, I.M., 2016. Rethinking the Role of Salps in the Ocean. Trends in Ecology & Evolution 31, 720–733. https://doi.org/10.1016/j.tree.2016.06.007

Hidalgo, M., Browman, H.I., 2019. Developing the knowledge base needed to sustainably manage mesopelagic resources. ICES Journal of Marine Science 76, 609–615. https://doi.org/10.1093/icesjms/fsz067

Hill Cruz, M., Kriest, I., Getzlaff, J., 2023. Diving deeper: Mesopelagic fish biomass estimates comparison using two different models. Front. Mar. Sci. 10, 1121569. https://doi.org/10.3389/fmars.2023.1121569

Jech, J.M., Horne, J.K., Chu, D., Demer, D.A., Francis, D.T.I., Gorska, N., Jones, B., Lavery, A.C., Stanton, T.K., Macaulay, G.J., Reeder, D.B., Sawada, K., 2015. Comparisons among ten models

of acoustic backscattering used in aquatic ecosystem research. The Journal of the Acoustical Society of America 138, 3742–3764. https://doi.org/10.1121/1.4937607

Jech, J.M., Lawson, G.L., Lowe, M.R., 2018. Comparing acoustic classification methods to estimate krill biomass in the Georges Bank region from 1999 to 2012: Georges Bank krill biomass. Limnology and Oceanography: Methods 16, 680–695. https://doi.org/10.1002/lom3.10275

Jones, B.A., Lavery, A.C., Stanton, T.K., 2009. Use of the distorted wave Born approximation to predict scattering by inhomogeneous objects: Application to squid. The Journal of the Acoustical Society of America 125, 73–88. https://doi.org/10.1121/1.3021298

Kaartvedt, S., Staby, A., Aksnes, D., 2012. Efficient trawl avoidance by mesopelagic fishes causes large underestimation of their biomass. Marine Ecology Progress Series 456, 1–6. https://doi.org/10.3354/meps09785

Klevjer, T.A., Martinez, Udane, Boyra, Guillermo, Røstad, Anders, Kaartvedt, Stein, Irigoien, Xabier, 2020. Integrated daytime EK60 echosounder data from Malaspina-2010 cruise. https://doi.org/10.1594/PANGAEA.923087

Kloser, R.J., Ryan, T., Sakov, P., Williams, A., Koslow, J.A., 2002. Species identification in deep water using multiple acoustic frequencies. Canadian Journal of Fisheries and Aquatic Sciences 59, 13.

Kloser, R.J., Ryan, T.E., Keith, G., Gershwin, L., 2016. Deep-scattering layer, gas-bladder density, and size estimates using a two-frequency acoustic and optical probe. ICES Journal of Marine Science 73, 2037–2048. https://doi.org/10.1093/icesjms/fsv257

Kloser, R.J., Ryan, T.E., Young, J.W., Lewis, M.E., 2009. Acoustic observations of micronekton fish on the scale of an ocean basin: potential and challenges. ICES Journal of Marine Science 66, 998–1006. https://doi.org/10.1093/icesjms/fsp077

Lavery, A.C., Wiebe, P.H., Stanton, T.K., Lawson, G.L., Benfield, M.C., Copley, N., 2007. Determining dominant scatterers of sound in mixed zooplankton populations. The Journal of the Acoustical Society of America 122, 3304–3326. https://doi.org/10.1121/1.2793613

Lawson, G.L., Wiebe, P.H., Ashjian, C.J., Gallager, S.M., Davis, C.S., Warren, J.D., 2004. Acoustically-inferred zooplankton distribution in relation to hydrography west of the Antarctic Peninsula. Deep Sea Research Part II: Topical Studies in Oceanography 51, 2041–2072. https://doi.org/10.1016/j.dsr2.2004.07.022

Lehodey, P., Conchon, A., Senina, I., Domokos, R., Calmettes, B., Jouanno, J., Hernandez, O., Kloser, R., 2015. Optimization of a micronekton model with acoustic data. ICES Journal of Marine Science 72, 1399–1412. https://doi.org/10.1093/icesjms/fsu233

Love, R.H., 1978. Resonant acoustic scattering by swimbladder-bearing fish. The Journal of the Acoustical Society of America 64, 571–580. https://doi.org/10.1121/1.382009

Lucca, B.M., Ressler, P.H., Harvey, H.R., Warren, J.D., 2021. Individual variability in sub-Arctic krill material properties, lipid composition, and other scattering model inputs affect acoustic estimates of their population. ICES Journal of Marine Science 78, 1470–1484. https://doi.org/10.1093/icesjms/fsab045

Lüdecke, D., 2018. ggeffects: Tidy Data Frames of Marginal Effects from Regression Models. Journal of Open Source Software 3, 772. https://doi.org/10.21105/joss.00772

Mackenzie, K.V., 1981. Nine-term equation for sound speed in the oceans. The Journal of the Acoustical Society of America, The Journal of the Acoustical Society of America 70, 807–812. https://doi.org/10.1121/1.386920

MacLennan, D.N., Fernandes, P.G., Dalen, J., 2002. A consistent approach to definitions and symbols in fisheries acoustics. ICES Journal of Marine Science 59, 365–369. https://doi.org/10.1006/jmsc.2001.1158

Mair, A.M., Fernandes, P.G., Lebourges-Dhaussy, A., Brierley, A.S., 2005. An investigation into the zooplankton composition of a prominent 38-kHz scattering layer in the North Sea. Journal of Plankton Research 27, 623–633. https://doi.org/10.1093/plankt/fbi035

Marohn, L., Schaber, M., Freese, M., Pohlmann, J.D., Wysujack, K., Czudaj, S., Blancke, T., Hanel, R., 2021. Distribution and diel vertical migration of mesopelagic fishes in the Southern Sargasso

863   Sea — observations through hydroacoustics and stratified catches. Mar. Biodivers. 51, 87.
864   https://doi.org/10.1007/s12526-021-01216-6

865   Marouchos, A., Sherlock, M., Kloser, R., Ryan, T., Cordell, J., 2016. A profiling acoustic and optical
866   system (pAOS) for pelagic studies; Prototype development and testing, in: OCEANS 2016 -
867   Shanghai. Presented at the OCEANS 2016 - Shanghai, IEEE, Shanghai, China, pp. 1–6.
868   https://doi.org/10.1109/OCEANSAP.2016.7485399

869   Mauchline, J., 1981. Measurement of body length of Euphausia superba Dana., in: BIOMASS
870   Handbook. pp. 4–9.

871   Mazerolle, M., 2023. AICcmodavg: Model selection and multimodel inference based on (Q)AIC(c). R
872   package version 2.3.2.

873   McClatchie, S., Thorne, R.E., Grimes, P., Hanchet, S., 2000. Ground truth and target identification for
874   fisheries acoustics. Fisheries Research 47, 173–191.

875   McFadden, D., 1973. Conditional logit analysis of qualitative choice behavior.

876   McGehee, D.E., O'Driscoll, R.L., Traykovski, L.V.M., 1998. Effects of orientation on acoustic scattering
877   from Antarctic krill at 120 kHz. Deep Sea Research Part II: Topical Studies in Oceanography
878   45, 1273–1294. https://doi.org/10.1016/S0967-0645(98)00036-8

879   Menkes, C., Allain, V., 2021. WARMALIS 1 cruise, Alis R/V. https://doi.org/10.17600/18000710

880   Olu, K., Allain, V., 2020. KANARECUP cruise, Alis R/V. https://doi.org/10.17600/18001103

881   Pakhomov, E., Yamamura, O., 2010. PICES Scientific Report No. 38 (No. 38). North Pacific Marine
882   Science Organization (PICES).

883   Pearre, S., 2003. Eat and run? The hunger/satiation hypothesis in vertical migration: history, evidence
884   and consequences. Biological Reviews of the Cambridge Philosophical Society 78, 1–79.
885   https://doi.org/10.1017/S146479310200595X

886   Peña, M., Andrès, L., González-Quirós, R., 2023. Target strength of *Cyclothone* species with fat-filled
887   swimbladers. Journal of Marine Systems 240, 103884.
888   https://doi.org/10.1016/j.jmarsys.2023.103884

889   Peña, M., Cabrera-Gámez, J., Domínguez-Brito, A.C., 2020. Multi-frequency and light-avoiding
890   characteristics of deep acoustic layers in the North Atlantic. Marine Environmental Research
891   154, 104842. https://doi.org/10.1016/j.marenvres.2019.104842

892   Peña, M., Villanueva, R., Escánez, A., Ariza, A., 2018. Opportunistic acoustic recordings of (potential)
893   orangeback flying squid Sthenoteuthis pteropus in the Central Eastern Atlantic. Journal of
894   Marine Systems 179, 31–37. https://doi.org/10.1016/j.jmarsys.2017.11.003

895   Perrot, Y., Brehmer, P., Habasque, J., Roudaut, G., Behagle, N., Sarré, A., Lebourges-Dhaussy, A.,
896   2018. Matecho: An Open-Source Tool for Processing Fisheries Acoustics Data. Acoustics
897   Australia 46, 241–248. https://doi.org/10.1007/s40857-018-0135-x

898   Proud, R., Cox, M.J., Brierley, A.S., 2017. Biogeography of the global ocean's mesopelagic zone.
899   Current Biology 27, 113–119. https://doi.org/10.1016/j.cub.2016.11.003

900   Proud, R., Handegard, N.O., Kloser, R.J., Cox, M.J., Brierley, A.S., Demer, D., 2019. From
901   siphonophores to deep scattering layers: uncertainty ranges for the estimation of global
902   mesopelagic fish biomass. ICES Journal of Marine Science 76, 718–733.
903   https://doi.org/10.1093/icesjms/fsy037

904   R Core Team, 2023. R: A Language and Environment for Statistical Computing. R Foundation for
905   Statistical Computing.

906   Receveur, A., Menkes, C., Allain, V., Lebourges-Dhaussy, A., Nerini, D., Mangeas, M., Ménard, F.,
907   2020a. Seasonal and spatial variability in the vertical distribution of pelagic forage fauna in
908   the Southwest Pacific. Deep Sea Research Part II: Topical Studies in Oceanography 175,
909   104655. https://doi.org/10.1016/j.dsr2.2019.104655

910   Receveur, A., Vourey, E., Lebourges-Dhaussy, A., Menkes, C., Ménard, F., Allain, V., 2020b.
911   Biogeography of micronekton assemblages in the natural park of the Coral Sea. Frontiers in
912   Marine Science 7, 449. https://doi.org/10.3389/fmars.2020.00449

913   Sarmiento-Lezcano, A.N., Olivar, M.P., Caballero, M.J., Couret, M., Hernández-León, S., Castellón, A.,
914   Peña, M., 2023. Swimbladder properties of *Cyclothone* spp. in the northeast Atlantic Ocean

915   and the Western Mediterranean Sea. Frontiers in Marine Science 10, 1093982.
916   https://doi.org/10.3389/fmars.2023.1093982

917 Scoulding, B., Chu, D., Ona, E., Fernandes, Paul.G., 2022. Erratum: ''Target strengths of two abundant
918   mesopelagic fish species". The Journal of the Acoustical Society of America 151, 3398–3398.
919   https://doi.org/10.1121/10.0011465

920 Scoulding, B., Chu, D., Ona, E., Fernandes, Paul.G., 2015. Target strengths of two abundant
921   mesopelagic fish species. The Journal of the Acoustical Society of America 137, 989–1000.
922   https://doi.org/10.1121/1.4906177

923 Scoulding, B., Gastauer, S., MacLennan, D.N., Fässler, S.M.M., Copland, P., Fernandes, P.G., Demer,
924   D., 2017. Effects of variable mean target strength on estimates of abundance: the case of
925   Atlantic mackerel (*Scomber scombrus*). ICES Journal of Marine Science 74, 822–831.
926   https://doi.org/10.1093/icesjms/fsw212

927 Sobradillo, B., Boyra, G., Martinez, U., Carrera, P., Peña, M., Irigoien, X., 2019. Target Strength and
928   swimbladder morphology of Mueller's pearlside (*Maurolicus muelleri*). Scientific Reports 9,
929   17311. https://doi.org/10.1038/s41598-019-53819-6

930 St. John, M.A., Borja, A., Chust, G., Heath, M., Grigorov, I., Mariani, P., Martin, A.P., Santos, R.S.,
931   2016. A dark hole in our understanding of marine ecosystems and their services: perspectives
932   from the mesopelagic community. Frontiers in Marine Science 3, 31.
933   https://doi.org/10.3389/fmars.2016.00031

934 Stanton, T., Wiebe, P.H., Chu, D., Benfield, M.C., Scanlon, L., Martin, L., Eastwood, L.R., 1994. On
935   acoustic estimates of zooplankton biomass. ICES Journal of Marine Science 51, 505–512.
936   https://doi.org/10.1006/jmsc.1994.1051

937 Stanton, T.K., Chu, D., Wiebe, P.H., 1998. Sound scattering by several zooplankton groups. II.
938   Scattering models. The Journal of the Acoustical Society of America 103, 236–253.
939   https://doi.org/10.1121/1.421110

940 Stanton, T., Chu, D., 2000. Review and recommendations for the modelling of acoustic scattering by
941   fluid-like elongated zooplankton: euphausiids and copepods. ICES Journal of Marine Science
942   57, 793–807. https://doi.org/10.1006/jmsc.1999.0517

943 Stanton, T.K., Sellers, C.J., Jech, J.M., 2012. Resonance classification of mixed assemblages of fish
944   with swimbladders using a modified commercial broadband acoustic echosounder at 1–6
945   kHz. Can. J. Fish. Aquat. Sci. 69, 854–868. https://doi.org/10.1139/f2012-013

946 Trenkel, V.M., Berger, L., Bourguignon, S., Doray, M., Fablet, R., Massé, J., Mazauric, V., Poncelet, C.,
947   Quemener, G., Scalabrin, C., Villalobos, H., 2009. Overview of recent progress in fisheries
948   acoustics made by Ifremer with examples from the Bay of Biscay. Aquatic Living Resources
949   22, 433–445. https://doi.org/10.1051/alr/2009027

950 Underwood, M.J., García-Seoane, E., Klevjer, T.A., Macaulay, G.J., Melle, W., 2020. An acoustic
951   method to observe the distribution and behaviour of mesopelagic organisms in front of a
952   trawl. Deep Sea Research Part II: Topical Studies in Oceanography 180, 104873.
953   https://doi.org/10.1016/j.dsr2.2020.104873

954 Underwood, M.J., Utne Palm, A.C., Øvredal, J.T., Bjordal, Å., 2021. The response of mesopelagic
955   organisms to artificial lights. Aquaculture and Fisheries 6, 519–529.
956   https://doi.org/10.1016/j.aaf.2020.05.002

957 Verma, A., Kloser, R.J., Duncan, A.J., 2017. Potential use of broadband acoustic methods for
958   micronekton classification. Acoustics Australia 45, 353–361. https://doi.org/10.1007/s40857-
959   017-0105-8

960 Warren, J.D., Smith, J.N., 2007. Density and sound speed of two gelatinous zooplankton: Ctenophore
961   (*Mnemiopsis leidyi*) and lion's mane jellyfish (*Cyanea capillata*). The Journal of the Acoustical
962   Society of America 122, 574–580. https://doi.org/10.1121/1.2739433

963 Williams, K., Rooper, C.N., De Robertis, A., Levine, M., Towler, R., 2018. A method for computing
964   volumetric fish density using stereo cameras. Journal of Experimental Marine Biology and
965   Ecology 508, 21–26. https://doi.org/10.1016/j.jembe.2018.08.001

966 Yasuma, H., Sawada, K., Takao, Y., Miyashita, K., Aoki, I., 2010. Swimbladder condition and target
967   strength of myctophid fish in the temperate zone of the Northwest Pacific. ICES Journal of
968   Marine Science 67, 135–144. https://doi.org/10.1093/icesjms/fsp218
969 Ye, Z., 1997. Low-frequency acoustic scattering by gas-filled prolate spheroids in liquids. The Journal
970   of the Acoustical Society of America 101, 1945–1952. https://doi.org/10.1121/1.418225
971 Young, J.W., Hunt, B.P.V., Cook, T.R., Llopiz, J.K., Hazen, E.L., Pethybridge, H.R., Ceccarelli, D., Lorrain,
972   A., Olson, R.J., Allain, V., Menkes, C., Patterson, T., Nicol, S., Lehodey, P., Kloser, R.J.,
973   Arrizabalaga, H., Anela Choy, C., 2015. The trophodynamics of marine top predators: Current
974   knowledge, recent advances and challenges. Deep Sea Research Part II: Topical Studies in
975   Oceanography 113, 170–187. https://doi.org/10.1016/j.dsr2.2014.05.015
976

31

Highlights

- Acoustic-trawl surveys in scattering layers of West tropical Pacific.

- Forward scattering models applied to micronekton trawl sampling with a high species diversity.

- The difference of volume scattering between echosounder and modelled from trawl is variable within scattering layers.

- Reduced disparities between acoustic and trawl data in night mesopelagic layers and in trawls capturing a high density of fish with swimbladders.

Declaration of interests

☒ The authors declare that they have no known competing financial interests or personal relationships that could have appeared to influence the work reported in this paper.

☐ The authors declare the following financial interests/personal relationships which may be considered as potential competing interests: